The Journal of Chemical Physics

RESEARCH ARTICLE | JULY 17 2026

# Auger spectra of thiouracils: Three molecules and four edges

Nayanthara K. Jayadev ; Dennis Mayer ; Florian Matz ; Fabiano Lever ; Lisa Mehner ; Constantin Walz ; Marta L. Murillo-Sánchez ; John Bozek ; Thomas-C. Jagau ; Markus Gühr ; Anna I. Krylov



*J. Chem. Phys.* 165, 034305 (2026)
https://doi.org/10.1063/5.0339155

The Journal of Chemical Physics ARTICLE pubs.aip.org/aip/jcp

# Auger spectra of thiouracils: Three molecules and four edges

Cite as: J. Chem. Phys. 165, 034305 (2026); doi: 10.1063/5.0339155
Submitted: 16 April 2026 • Accepted: 1 July 2026 •
Published Online: 17 July 2026



Nayanthara K. Jayadev,[1] Dennis Mayer,[2] Florian Matz,[3] Fabiano Lever,[2] Lisa Mehner,[4] Constantin Walz,[4] Marta L. Murillo-Sánchez,[5] John Bozek,[6] Thomas-C. Jagau,[3] Markus Gühr,[2,7] and Anna I. Krylov[1,a)]

## AFFILIATIONS

[1] Department of Chemistry, University of Southern California, Los Angeles, California 90089, USA
[2] Deutsches Elektronen-Synchrotron DESY, 22607 Hamburg, Germany
[3] Department of Chemistry, KU Leuven, B-3001 Leuven, Belgium
[4] Department of Physics and Astronomy, University of Potsdam, 14476 Potsdam, Germany
[5] May-Planck-Institut für Kernphysik, 69117 Heidelberg, Germany
[6] Synchrotron SOLEIL, 91190, Saint-Aubin, France
[7] Department of Physical Chemistry, University of Hamburg, 20146 Hamburg, Germany

[a)] **Author to whom correspondence should be addressed:** krylov@usc.edu

## ABSTRACT

This study presents a comprehensive investigation of the Auger spectra of three thionated uracils using a combination of theory and experiment. Non-resonant Auger spectra measured at the K-edges of carbon, nitrogen, and oxygen, as well as at the $L_{2,3}$ edge of sulfur, are reported. Even though the final decay states (valence two-hole states) are the same for all edges, the resulting Auger spectra are strikingly different, highlighting the local nature of the Auger decay. Theoretical modeling, which employed a series of approaches incorporating varying levels of correlation and different treatments of the metastable states, provides a clear interpretation of the experimental spectra. The analysis highlights the crucial role of electron correlation, evident in both the density of the decay states and the spectra constructed using channel-specific partial decay widths, as well as the importance of spin–orbit coupling in shaping the L-edge spectra of thiouracils.



## I. INTRODUCTION

Auger decay is a non-radiative process in which a core-vacancy state decays by filling the hole and ejecting an electron (Auger electron) into the continuum. Auger spectra are obtained by recording the yield of Auger electrons as a function of their kinetic energies. The energies of the Auger electrons correspond to the differences between the energies of the initial core-ionized state (or a core-excited state in the case of resonant Auger decay) and the final decay states, which are doubly ionized valence states (or singly ionized valence states in the case of resonant Auger decay). The intensities of the peaks are proportional to the partial decay rates of the respective channels, which, in turn, are proportional to the decay widths.

*Ab initio* calculations of Auger spectra are challenging because of the difficulties with computing core-vacancy states due to their metastable character and the continuum nature of the Auger electron. Hence, in order to compute energies of these states and their decay rates, one needs to incorporate the autoionization continuum in quantum-chemistry treatments. The core–valence separation (CVS) approach,[1] which allows one to decouple the core-level states from the valence ionization continuum, is an effective way to describe the core-level states. The combination of CVS with the equation-of-motion (EOM) coupled-cluster (CC) framework[2–4] has been successfully used to compute energies of core-level states and their spectroscopic signatures.[5–15]

Previous theoretical studies of Auger decay have explored a variety of approaches, ranging from assuming equal decay rates for all channels[16,17] to methods based on non-Hermitian extensions of quantum mechanics designed for resonances,[18] such as complex-variable approaches[19,20] and techniques using different

representations of the continuum. The latter approaches include discretized continuum treatment via Stieltjes imaging[21–23] and explicit treatment of free-electron states within the Feshbach–Fano (FF) ansatz.[24–39] Within the FF framework, the continuum state can be effectively represented by a one-center approximation (OCA).[28,40–45]

Within EOM-CC, there are two approaches for computing decay rates of core-level states—one based on the FF formalism[46–49] and another based on the complex basis functions (CBF) formalism.[19,20,50–52]

In the FF framework, the decay rates are computed using Wentzel's ansatz,[53] an expression akin to the Fermi golden rule. The decay rate $\Gamma_{\mu n}$ of the initial core-vacancy state $n$ into the final two-hole ($2h$) state $\mu$ is given by a matrix element between the initial core-vacancy state ($\Psi_n^{IP}$) and the final decay state, a product of the doubly ionized valence state ($\Psi_\mu^{DIP}$) and a free-electron state ($\Psi_{\mathbf{k}}^{el}$),

$$\Gamma_{\mu n} = 2\pi g_\alpha \int d\Omega_{\mathbf{k}} \left[ \langle \Psi_n^{IP} | H | \Psi_\mu^{DIP} \times \Psi_{\mathbf{k}}^{el} \rangle \langle \Psi_\mu^{DIP} \times \Psi_{\mathbf{k}}^{el} | H | \Psi_n^{IP} \rangle \right], \quad (1)$$

where $\mathbf{k}$ is the momentum of the emitted electron (the absolute value of $\mathbf{k}$ is determined by the energy difference between the core–hole and decay states), factor $g_\alpha$ accounts for spin degeneracy, and the integration is done over all directions of $\mathbf{k}$.

In the CBF approach, Auger decay is modeled as a two-step procedure akin to Wentzel's ansatz. The partial decay rates are computed from the imaginary part of the energy of the core-vacancy state, either by an *a posteriori* decomposition of the imaginary energy in terms of the decay channels[20,52] or by applying channel-specific projectors.[19] These procedures yield the decay rates in terms of orbital pairs of the initial-state wave function, which are then mapped onto the final states in a second step.[54]

Recently, these two approaches have been used to model the Auger spectrum of benzene, showing remarkably good agreement with each other and with experiments.[55,56] FF and CBF treatments have also been applied to model $L_{2,3}$-edge spectra, where inclusion of spin–orbit interactions is important for quantitative accuracy[57] by using the state-interaction framework[58,59] with spin–orbit couplings (SOCs) computed as matrix elements of the Breit–Pauli Hamiltonian.[60–62]

In this contribution, we present a combined experimental and theoretical study on the Auger spectra of the three thionated nucleobases shown in Fig. 1: 2- and 4-thiouracils (2TU and 4TU, respectively) as well as 2,4-dithiouracil (2,4dTU). Thionated nucleobases are important in biology and medicine.[63–66] They were found in tRNA (translational RNA) of many bacteria, yeasts, and even higher organisms[63] and are believed to modulate the rate and fidelity of the mRNA (messenger RNA) decoding process, thereby effecting changes in the metabolism of the organisms. Sulfur-substituted nuclear bases have also been explored in the context of artificial self-replicating cells in which the genetic content encoded in RNA-like polymers is replicated without the enzymes,[64] as likely occurred in prebiotic chemistry. In medicine, thionated nucleobases and related molecules are used as immunosuppressants and anticancer photodynamic therapeutic agents. The thionated uracils are also finding applications as UV cross-linking agents.[67] Many of these applications are based on the unique photochemistry of thionated nucleobases.[65,66] For example, UV-excited thiouracils exhibit ultrafast relaxation into highly reactive triplet states with a high quantum yield.[65,66,68,69] In our own study, we investigated the details of UV-induced electronic relaxation using x-ray induced Auger and core–photoelectrons as well as x-ray absorption.[70–74] We also used Coulomb-explosion imaging to correlate the electronic dynamics with molecular structural rearrangements.[75]

Thionated nucleobases are also interesting from the fundamental point of view. Owing to their heteronuclear nature, these molecules can interact with x-rays in several distinct energy regimes. Here, we report Auger spectra corresponding to the ionization at the carbon, nitrogen, and oxygen K-edges as well as sulfur's L-edge. The decay states, which correspond to the valence $2h$ states, are independent of the initial core–hole state; however, the intensities for each decay channel depend on the edge, illuminating the local nature of the Auger process. The differences between the three molecules are also interesting, as they reveal the effect of the molecular structure on the spectra.

From the theoretical side, we present and compare theoretical Auger spectra computed using different treatments ranging from assuming uniform intensities of each decay channel—in other words, simply taking the density of states (DOS)—to spectra in which the channel intensities are computed with the FF and CBF approaches. We also investigate the impact of different treatments of electron correlation as well as relativistic effects. Given that the theoretical treatment of core-vacancy states and Auger decay is an active area of research, the availability of reliable experimental data is crucially important for validating different theoretical frameworks, and our contribution provides such data for three molecules and four edges, building upon our previous studies of thiouracils.[70–74]

The outline of the paper is as follows. In Sec. II, we present the theoretical framework and computational details. The experimental details are given in Sec. III. In Sec. IV, we first discuss the K-edge spectra, focusing on the effects of correlation on the energies and

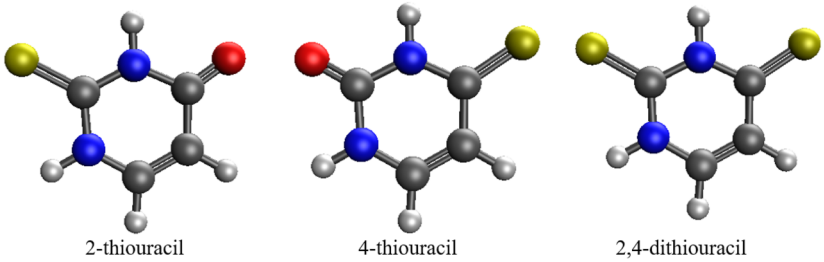


**FIG. 1.** Structures of the thionated uracils. Color code: Dark gray (carbon), blue (nitrogen), red (oxygen), yellow (sulfur), and light gray (hydrogen).

decay rates, and then focus on the sulfur L-edge spectra, where we also discuss different treatments of the continuum and relativistic effects. Our concluding remarks are given in Sec. V.

## II. THEORETICAL FRAMEWORK AND COMPUTATIONAL DETAILS

### A. Initial core-ionized states, decay states, and density of states

The energies of the initial core–hole and the decay states ($2h$ valence states) can be crudely estimated using Koopmans' theorem. For a more accurate treatment, we use EOM-CCSD methods in which the states of interest are found by diagonalizing the similarity-transformed Hamiltonian, $\bar{H} = e^{-T} H e^{T}$, in the appropriate sector of the Fock space. Here, $T$ denotes the coupled-cluster amplitudes of the reference state.[2–4] Core-ionized states are described by EOM-CCSD for ionization potentials combined with CVS (CVS-EOM-IP-CCSD),[5–9] and the decay states are described by several flavors of EOM-CC for double ionization potentials (EOM-DIP-CC).

The number of decay channels is given by the product of the number of initial core-ionized states and $2h$ (or DIP) states. Since for each edge the energies of the initial core–hole states span a very narrow range, the spread of the energies of the Auger electrons reflects the DOS of the decay states. Hence, the analysis of the decay states provides the basis for the interpretation of the Auger spectra. We employ a hierarchy of theoretical approaches to compute the DOS of the $2h$ states. The theoretical approaches are as follows:

- A Koopmans treatment in which the DOS is computed from the Hartree–Fock orbital energies. Note that this approach does not distinguish between triplet and singlet states.
- EOM-DIP-CCSD($2h$) calculations in which the DIP energies are obtained by diagonalizing the similarity-transformed Hamiltonian, $\bar{H}$, in the space of $2h$ determinants.
- EOM-DIP-CCSD($2h$) calculations with a perturbative account of contributions from $3h1p$ determinants; this is accomplished by preconverging $2h$ states and then making one Davidson iteration in the full space.
- Full EOM-DIP-CCSD calculations in which $\bar{H}$ is diagonalized in the space of $2h$ and $3h1p$ determinants.

### B. From DOS to Auger spectra

To proceed from the DOS to the Auger spectra, we use several approaches of increasing complexity.

In the simplest treatment, we use orbital energies to compute the energies of the initial and final decay states. We then construct the Auger spectra either by assigning equal intensities to all decay channels or by weighting each channel according to Mulliken's population of the valence molecular orbitals (MOs) on the atoms hosting the initial core–hole.

Using Mulliken-like populations to assign intensities to each decay channel is based on the assumption that Auger decay is dominated by local valence-to-core transitions. We note that this reasoning was used in an early study of the Auger spectra of small molecules.[76] For each decay channel, we compute the weight of the corresponding valence MOs on the respective atoms (e.g., carbons for carbon K-edge, nitrogens for nitrogen K-edge, etc.). Mulliken's population analysis is based on the following property of the density matrix,

$$N = \sum_{\mu\nu} \gamma_{\mu\nu} S_{\mu\nu} = \sum_{\mu} (\gamma S)_{\mu\mu} = \mathrm{Tr}[\gamma S], \tag{2}$$

where $N$ is the total number of electrons and $\gamma$ and $S$ are, respectively, the density and overlap matrices in the atomic orbital (AO) basis. The population on a specific atom is given by the trace of a submatrix over all AOs belonging to that atom. For example, if we are looking at the population on the oxygen atom,

$$P(O) = \sum_{\mu\nu \in O} \gamma_{\mu\nu} S_{\mu\nu}. \tag{3}$$

For a given atomic edge, we use Mulliken's population of the valence MOs, corresponding to a particular decay state, associated with the specific atoms with the core–hole as a proxy for their contribution to the decay process. This approach affords a quick qualitative evaluation of the Auger spectra, as it reflects the spatial proximity of the initial core-ionized state and the relevant valence orbitals of the decay channels. These calculations can be carried out as postprocessing of the quantum-chemistry calculations using *Python* scripts, which are now included in the *ezAuger* suite.[77] As we show below, the so-computed spectra provide a reasonable zero-order description of the Auger spectra. Importantly, they cover the full range of energies of the Auger electrons. However, because these calculations do not include correlation effects, the absolute energies are off and the fine details of the spectra are not captured. Moreover, for the $L_{2,3}$ edge, Mulliken's populations do not capture the extent of alignment between the core–hole and valence–hole states. Therefore, while the Koopmans' approach can serve as a quick qualitative tool for analyzing Auger spectra, more accurate correlated methods are required for quantitative analysis.

Toward this end, we employ approaches based on EOM-CCSD wave functions and the FF[46,47] and CBF[19,20,50,51] formalisms for computing partial decay widths. In the FF approach, the decay rate is given by Eq. (1). By integrating over $N-2$ electron coordinates,[46] the requisite matrix elements become

$$\begin{aligned}
\langle \Psi_n^{IP} | H | \Psi_\mu^{DIP} \times \Psi_{\mathbf{k}}^{el} \rangle &= \sum_p h_{p\mathbf{k}} \times {}^{n\mu} d^p + \frac{1}{2} \sum_{pqr} \langle pq \| \mathbf{k}r \rangle \times {}^{n\mu} D_r^{pq}, \\
\langle \Psi_\mu^{DIP} \times \Psi_{\mathbf{k}}^{el} | H | \Psi_n^{IP} \rangle &= \sum_p h_{\mathbf{k}p} \times {}^{\mu n} d_p + \frac{1}{2} \sum_{pqr} \langle \mathbf{k}r \| pq \rangle \times {}^{\mu n} D_{pq}^r,
\end{aligned} \tag{4}$$

where $h_{p\mathbf{k}}$ and $\langle pq \| \mathbf{k}r \rangle$ are matrix elements of the one-electron and two-electron parts of the Hamiltonian, indices $p, q, r$ run over molecular orbitals, and $\mathbf{k}$ now also denotes the continuum orbital. The integrals are contracted with one- and two-body Dyson amplitudes,[46,78] ${}^{n\mu} d^p$ and ${}^{n\mu} D_r^{pq}$,

$${}^{n\mu} d^p = \langle \Psi_n^N | p^\dagger | \Psi_\mu^{N-1} \rangle, \quad {}^{\mu n} d_p = \langle \Psi_\mu^{N-1} | p | \Psi_n^N \rangle, \tag{5}$$

and

$${}^{n\mu} D_r^{pq} = \langle \Psi_n^N | p^\dagger q^\dagger r | \Psi_\mu^{N-1} \rangle, \quad {}^{\mu n} D_{qr}^p = \langle \Psi_\mu^{N-1} | p^\dagger q r | \Psi_n^N \rangle. \tag{6}$$

There are two sets of one- and two-particle Dyson amplitudes because of the non-Hermitian nature of EOM-CC theory.[3,79,80] The contributions due to one-body Dyson orbitals are small, owing to the two-electron nature of the Auger decay. The application of the FF approach requires an explicit free-electron state, which can be approximated by a plane wave or a Coulomb wave.

In the CBF approach,[50,51,81–84] Auger decay is described using an $L^2$-representation of the resonance wave function obtained via analytical continuation of the Hamiltonian into the complex plane. Therefore, the CBF approach does not require an explicit description of the Auger electron. The complex resonance energy is determined as an eigenvalue of a non-Hermitian Hamiltonian, with the real part describing the energy of a resonance and the imaginary part describing its width. The total decay width is then

$$\Gamma = -2\,\mathrm{Im}(E_{\mathrm{res}}). \tag{7}$$

To obtain partial widths for each channel, we employ the Auger channel projector (ACP) approach, in which partial widths are computed by applying channel-specific projectors.[19] The projectors are constructed by removing a particular set of determinants corresponding to the final decay state from the many-body expansion, akin to the CVS projectors (out-ACP). Alternatively, the set of determinants corresponding to the final decay state can be added to the CVS-EOM-IP-CCSD wave function (in-ACP). Then the partial widths can be computed as the difference between the calculations with and without the inclusion of a particular channel-specific set of determinants.

For the nitrogen and oxygen K-edges, we use the FF method with the continuum electron described as a plane wave (FF-PW). According to our recent benchmarks, this approximation performs poorly for $L_{2,3}$-edge Auger spectra[57] for which a Coulomb-wave representation of the continuum state (FF-CW) provides a more accurate description of the partial decay widths. The CW treatment is based on the pseudo-partial-wave expansion in terms of products of a plane wave and Gaussian functions, as described elsewhere.[46] The center of the Coulomb wave is placed on the atom bearing the core hole, i.e., sulfur. For all three thiouracils, we employ a uniform effective charge $Z_{eff}$ = 6.7 for all channels, the same value as used for $H_2S$ in our recent study.[57]

For the S L-edge spectra, we compare the results obtained with the FF-CW and CBF approaches. Here, we also include SOC, which has a significant effect on the energies and partial decay widths of the Auger electrons. SOC arises from relativistic interactions between the electron's intrinsic magnetic moment (spin) and the magnetic field generated by the motion of charged particles (electrons orbiting the nuclei). It mixes states of different spin multiplicities, which are uncoupled in a purely non-relativistic framework, and leads to the energetic splitting of orbitals with non-zero orbital angular momentum. In particular, SOC splits the atomic $2p$ orbitals into the $2p_{1/2}$ and $2p_{3/2}$ components, giving rise to two distinct edges in the L-edge spectra: $L_2$ and $L_3$. The degeneracy of the $2p_{1/2}$ and $2p_{3/2}$ levels can be further lifted by the molecular field arising from an anisotropic chemical environment. We evaluate SOC-perturbed energies and partial decay widths using the state-interaction approach,[58,59] as in our previous studies.[57,60,62] For the core-ionized states, the state-interaction calculations include six ($2p^{-1}$) states; for 2,4dTU, the model Hamiltonian is diagonalized separately for each of the two non-equivalent S atoms.

### C. Computational details

We carried out the calculations using equilibrium geometries of the thionated uracils optimized at the RI-MP2/cc-pVTZ level of theory. Relevant Cartesian coordinates are provided in the supplementary material.

Within the Koopmans approach, we computed DOS from the Hartree–Fock orbital energies. We then calculated the singlet and triplet DIP states (120 in each multiplicity) using EOM-DIP-CCSD($2h$) and including the perturbative correction to account for the effect of the $3h1p$ determinants. We also performed full EOM-DIP-CCSD calculations, in which we were able to compute 60 singlet and 60 triplet states.

For the N and O K-edges, we used the 6-311(2+,+)G** basis with an uncontracted core.[85] For the S $L_{2,3}$ edge, we used the 6-311G basis on C, N, O, and H and the 6-311G(2df) basis with uncontracted core functions on S.

In the CBF calculations, we employed the in-ACP approach[19] using the cc-pCVTZ(5sp) real basis set for S, cc-pCVTZ for C, N, and O, and cc-pVTZ for H. The cc-pCVTZ(5sp) basis set was constructed by replacing the valence $s$- and $p$-shells in the standard cc-pCVTZ basis with those from the cc-pCV5Z basis.[19,20] In addition, a set of $4s4p4d$ diffuse complex functions was placed on the sulfur atom. Within the in-ACP framework, the partial Auger decay widths are obtained by weighting each channel by the square of the corresponding excitation amplitude in the EOM-DIP-CCSD wave function associated with the final $2h$ state.[19,20]

To generate the Auger spectra from the computed energies and decay widths, we convoluted the stick spectra with a Gaussian function. Unless specified otherwise, we used Gaussian functions with a full width at half maximum (FWHM) of 0.70 eV.

All electronic structure calculations were carried out using the *Q-Chem* package.[86,87] Auger spectra were generated using the *ezAuger* suite.[77]

## III. EXPERIMENTAL DETAILS

The experimental Auger spectra were taken at the PLEIADES beamline of the synchrotron SOLEIL.[88] The experimental setup was identical to recently published x-ray photoelectron experiments on these molecules.[73] In short, a heatable gas cell inside the vacuum chamber was used to evaporate the samples at temperatures around 120 °C, resulting in vapor pressures on the order of $1 \times 10^{-4}$ mbar.[89] The beamline uses an Apple II HU 80 permanent magnet undulator to create the x-rays. The photon energy was selected with a 600 lines/mm grating. Pinholes at both sides of the gas cell allowed the beam to enter and exit. The focal size inside the cell was $100 \times 250\ \mu m^2$, where the vertical dimension is an image of the monochromator slit. The photon flux for the slit size was $\sim 2 \times 10^{13}$ photons/s. Photon energies of 610, 430, 320, and 250 eV for 2TU and 628, 495, 382, and 250 eV for 4TU and 2,4dTU were used to core-ionize the samples. The hemispherical electron kinetic energy analyzer (Scienta R4000) was used to collect the Auger electrons within the expected kinetic energy ranges. The pass energy for the hemispherical analyzer was 200 eV such that the resolution was 250 meV.

## IV. RESULTS AND DISCUSSION

Figure 2 presents the experimental Auger spectra of the thionated uracils at the K-edges of C, N, and O as well as the $L_{2,3}$-edge of S. The energies of the Auger electrons produced from the four edges are well separated. The carbon K-edge spectra of the three molecules span the range of 220–280 eV and appear broad and unstructured. Only 2,4dTU shows a sharp rise at 265 eV. The peaks at around 230 eV in 2TU and 4TU originate from 2nd-order undulator radiation and show the N and O 1*s* photoline, respectively. Similarly, the K-edge spectra of N are broad, spanning the 330–390 eV range. However, they show slightly more structure, exhibiting at least two distinguishable peaks at 370 and 375 eV. At the O K-edge, the spectra display more pronounced structure. In both 2TU and 4TU, an intense band appears between 495 and 510 eV, followed by a decline in intensity between 480 and 495 eV, and then a weaker band in the 470–480 eV range. The K-edge spectra are similar across the three molecules. Overall, the K-edge spectra span ~60 eV, consistent with the expected distribution of decay states, which we describe in detail below.

The Auger spectra at the S $L_{2,3}$-edge have better-resolved structure, spanning a narrower energy range of 135–150 eV. In comparison to the other edges, the differences between the three molecules are more pronounced at this edge. Below, we focus on the effect of the second sulfur atom in 2,4dTU relative to 2TU and 4TU.

We are not reporting the $L_1$ edge Auger spectra because of the strong overlap of $L_1$ and $L_{2,3}$, which results in very fast Coster–Kronig decays between the two subshells. Moreover, the low kinetic energy of the emitted valence electrons (<60 eV) from this decay impedes a clean detection of the spectra because it repeatedly overlaps with other (much stronger) core-level photolines.

### A. Molecular orbital framework

Figures 3–5 show the occupied valence MOs for the three thiouracils, and Tables S1–S3 in the supplementary material give the corresponding orbital energies and combined Mulliken's populations on the S, O, N, and C atoms.

Each molecule has 21 occupied valence MOs. We classify these MOs as outer-, mid-, and inner-valence MOs according to their Koopmans ionization energies: the first seven MOs (9–15 eV) form the outer-valence region, the next seven MOs (16–22 eV) form the mid-valence region, and the last seven MOs (23–39 eV) form the inner-valence region. This classification is similar to that of Moddeman *et al.*,[76] who divided valence electrons into strongly and weakly bound groups, the former associated with orbitals with large 2*s* contributions and the latter associated with orbitals with large 2*p* contributions.

In 2TU (Fig. 3) and 4TU (Fig. 4), the outer-valence region comprises the orbitals from the HOMO ($6a''$) to HOMO-6 ($3a''$).

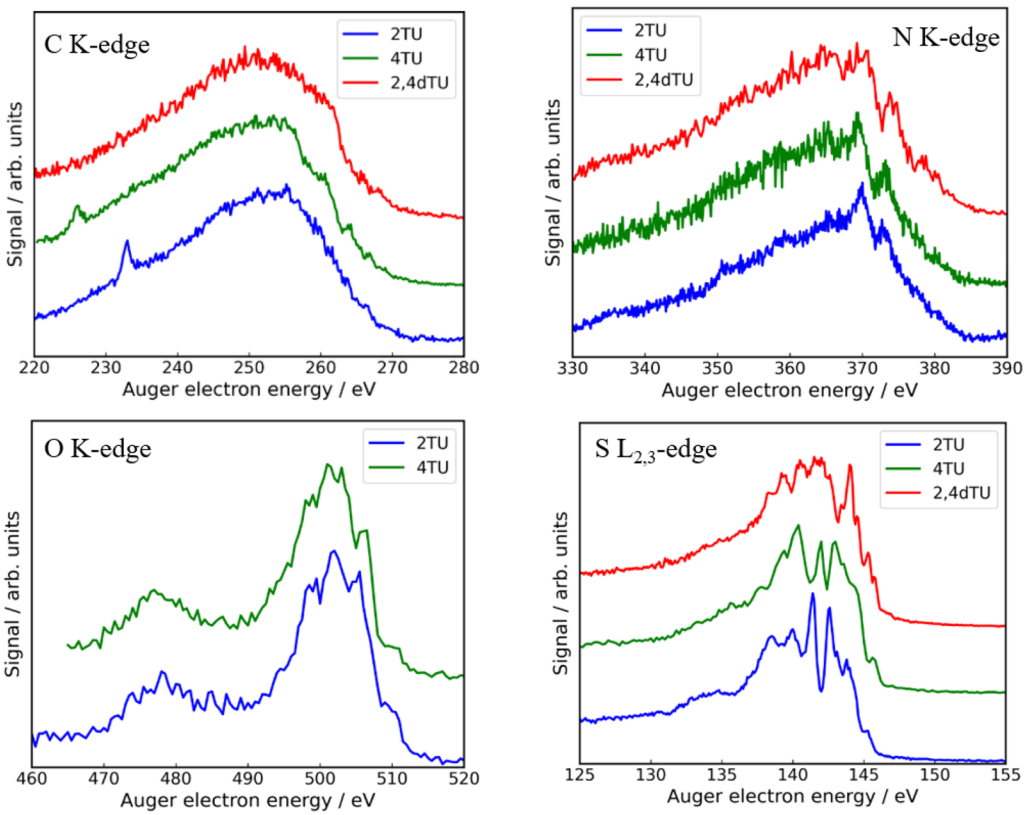


**FIG. 2.** Thiouracils: Experimental Auger spectra at the C, N, O K-edges, and S $L_{2,3}$-edge.

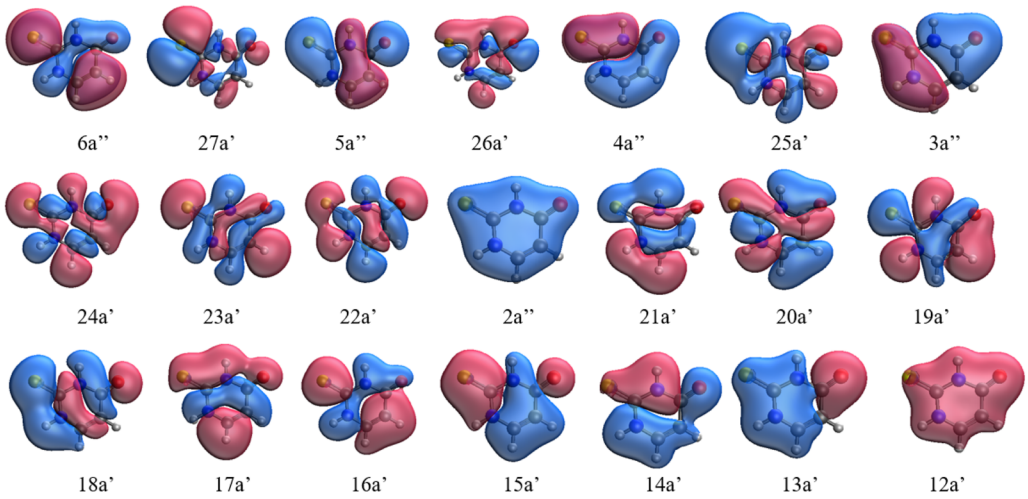


**FIG. 3.** Occupied molecular orbitals of 2-thiouracil. Orbitals are numbered from the bottom up sequentially in each irrep. The outer-valence group comprises orbitals from 6$a''$ (HOMO) to 3$a''$ (HOMO-6), the mid-valence group comprises orbitals from 24$a'$ (HOMO-7) to 19$a'$ (HOMO-13), and the inner-valence group comprises orbitals from 18$a'$ (HOMO-14) to 12$a'$ (HOMO-20).

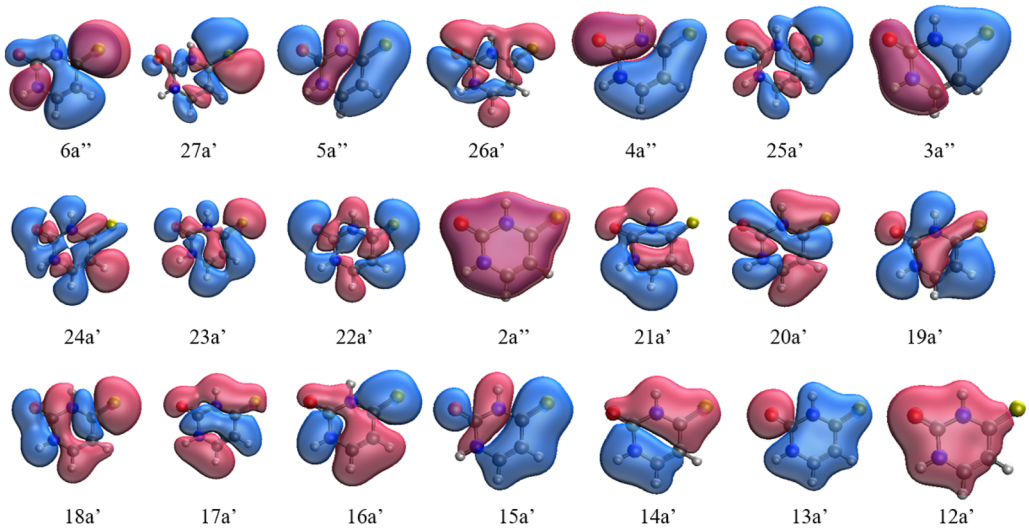


**FIG. 4.** Occupied molecular orbitals of 4-thiouracil. Orbitals are numbered from the bottom up sequentially in each irrep. The outer-valence group comprises orbitals from 6$a''$ (HOMO) to 3$a''$ (HOMO-6), the mid-valence group comprises orbitals from 24$a'$ (HOMO-7) to 19$a'$ (HOMO-13), and the inner-valence group comprises orbitals from 18$a'$ (HOMO-14) to 12$a'$ (HOMO-20).

Among these, the 6$a''$, 27$a'$, and 25$a'$ orbitals are localized on the sulfur atom, whereas the 5$a''$, 26$a'$, and 3$a''$ orbitals have substantial density on oxygen. Nearly all orbitals have significant weights on the carbon atoms, followed by the weights on the nitrogens. In contrast, 2,4dTU (Fig. 5) contains two S atoms, whose combined Mulliken's populations dominate across all outer-valence MOs (7$a''$–3$a''$). In all three molecules, no MOs in the mid-valence region have substantial Mulliken's populations on S. Instead, these orbitals have large contributions from the C and N atoms, with a few orbitals showing contributions from O. We observe a similar trend in the inner-valence region, where only a few MOs have notable populations on sulfur or oxygen. Below, we demonstrate how Mulliken's populations help interpret the shapes of the Auger spectra at each edge.

We first compute DOS spectra within the Koopmans framework, where the energies of the 2$h$ states are given by the sum of the corresponding orbital energies. This results in 21 decay states corresponding to the removal of both electrons from the same valence

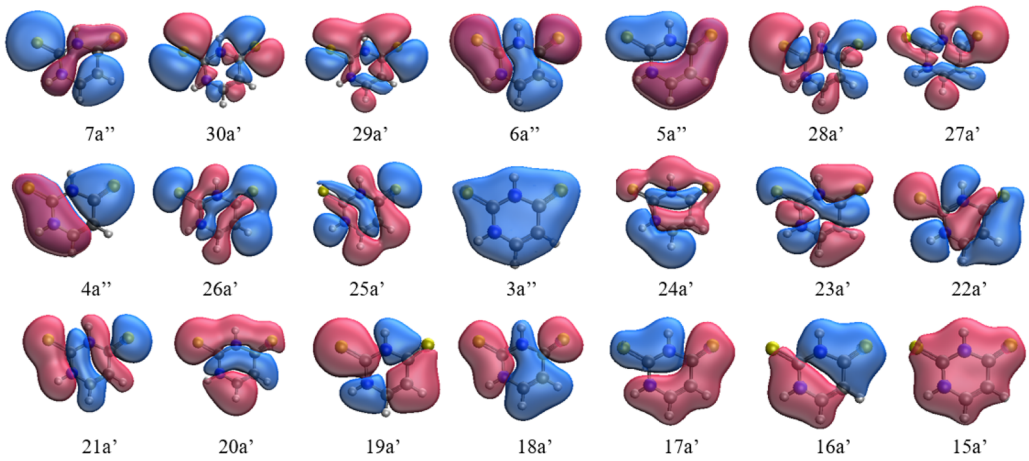


**FIG. 5.** Occupied molecular orbitals of 2,4-dithiouracil. Orbitals are numbered from the bottom up sequentially in each irrep. The outer-valence group comprises orbitals from 7*a*′′ (HOMO) to 27*a*′ (HOMO-6), the mid-valence group comprises orbitals from 4*a*′′ (HOMO-7) to 22*a*′ (HOMO-13), and the inner-valence group comprises orbitals from 21*a*′ (HOMO-14) to 15*a*′ (HOMO-20).

MO and an additional 210 decay states arising from the removal of electrons from two different MOs.

Figure 6 shows the Koopmans DOS. In these calculations, we computed all main decay states, which span the energy range between 18 and 78 eV. This is close to the 60 eV spanned in the experimental K-edge Auger spectra shown in Fig. 2. The Koopmans DOS is relatively unstructured and similar in the three molecules. The peaks below 20 eV originate exclusively from the outer-valence MOs. At higher energies, numerous peaks emerge, reflecting the increased number of available 2*h* states. In the 20–40 eV region, the decay states correspond to combinations of outer-outer, outer–mid, mid–mid, and outer–inner valence ionizations, leading to a large DOS. At even higher energies, decay states of mid–mid, mid–inner, and inner–inner character appear, with the number of decay states gradually decreasing. Notably, most of the states at energies ≥60 eV arise from the removal of the electrons from inner-valence MOs. The inner–inner decay states span nearly 18 eV and are well-separated in energy, resulting in fewer states contributing to each peak within this region.

### B. The effect of correlation on the energies of the decay states: EOM-DIP-CCSD vs Koopmans approach

Although Koopmans DIP energies span the full experimental range, the corresponding DOS do not account for electron correlation. To go beyond the Koopmans framework, we employ correlated methods for computing the decay states. In particular, we compare the Koopmans DOS with the results obtained from two variants of EOM-DIP-CCSD: calculations restricted to 2*h* determinants [EOM-DIP-CCSD(2*h*)] and calculations including both 2*h* and 3*h*1*p* determinants [full EOM-DIP-CCSD or EOM-DIP-CCSD(2*h*, 3*h*1*p*)]. Unfortunately, when using higher levels of correlation, we can only compute a subset of the decay channels due to convergence problems.

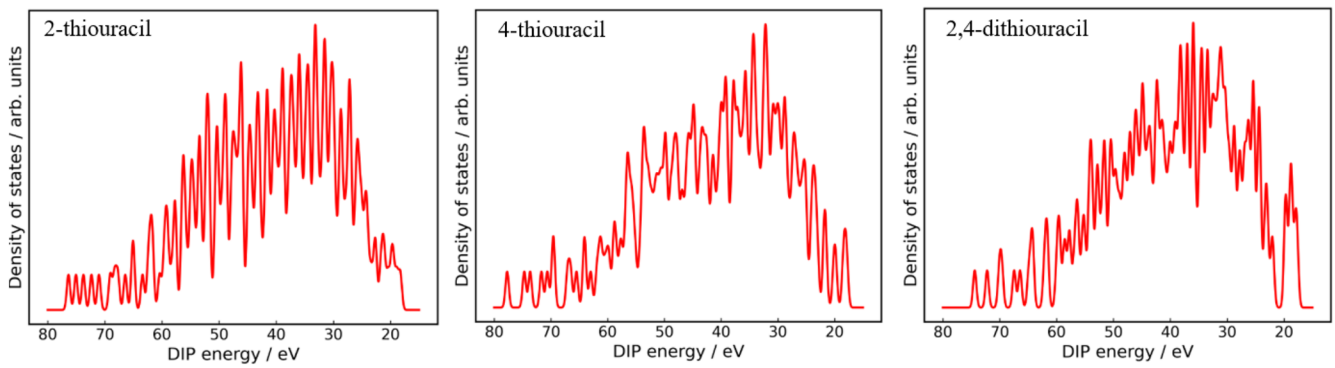


**FIG. 6.** Thiouracils: The density of 2*h* states computed using Koopmans' theorem.

Figures 7 and S1 in the supplementary material compare the density of states (DOS) obtained using the Koopmans, EOM-DIP-CCSD$(2h)$, and EOM-DIP-CCSD$(2h,3h1p)$ approaches. The energy ranges covered by each method are indicated in Fig. 7 by shaded regions. Using EOM-DIP-CCSD$(2h)$, we computed 120 singlet and 120 triplet states spanning the 25–55 eV energy range, corresponding to a window of ~30 eV. In the Koopmans spectra (first row), the blue-shaded region highlights the portion of the total Koopmans energy range that is accessible within the EOM-DIP-CCSD$(2h)$ framework, which amounts to nearly half of the full range.

In contrast, EOM-DIP-CCSD$(2h,3h1p)$ yields 60 singlet and 60 triplet states spanning a narrower energy interval of 23–35 eV, corresponding to a window of ~12 eV. This range is shaded in green in the first and second rows of Fig. 7. Overall, the EOM-DIP-CCSD$(2h,3h1p)$ treatment covers roughly one-sixth of the Koopmans energy range and less than half of that accessible with EOM-DIP-CCSD$(2h)$.

Figure S1 in the supplementary material presents the DOS plots shifted to align their respective energy onsets with those obtained from full EOM-DIP-CCSD; the applied shifts are indicated in the figure. As anticipated, the Koopmans treatment underestimates double-ionization energies, while EOM-DIP-CCSD$(2h)$ systematically overestimates them relative to the full EOM-DIP-CCSD calculations.

Interestingly, the differences in the DOS among the three molecules are more pronounced at the correlated levels. The inclusion of correlation changes the energies of the valence $2h$ states in a

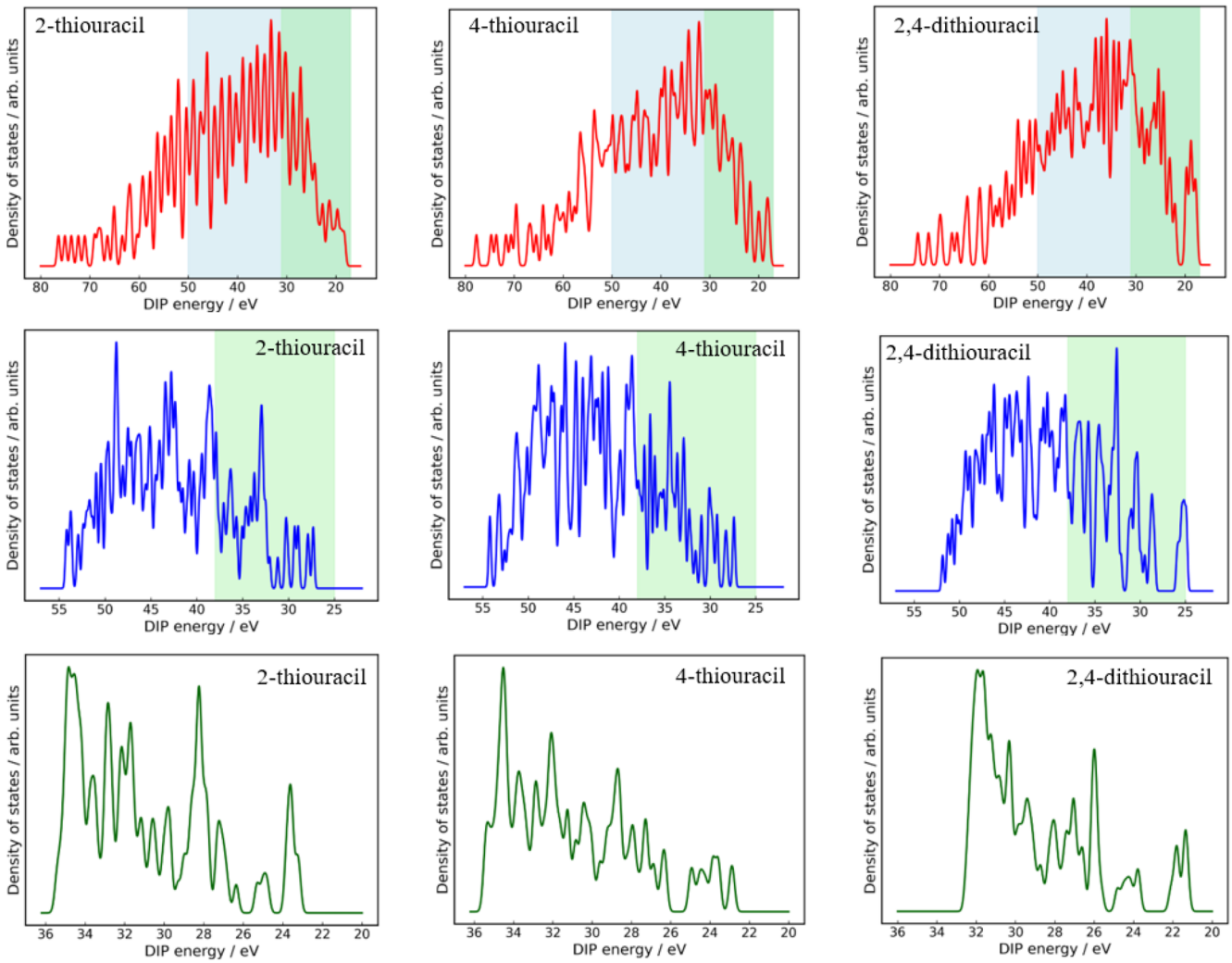


**FIG. 7.** Thiouracils: The density of $2h$ states computed using Koopmans' approach (first row), EOM-DIP-CCSD$(2h)$ (second row), and EOM-DIP-CCSD$(2h,3h1p)$ (third row).

way that changes the shape of the DOS. Already at the EOM-DIP-CCSD($2h$) level, the spectra acquire additional structure. Notably, an energy gap appears at 26–28 eV in 2,4dTU. With the improved treatment of correlation in full EOM-DIP-CCSD, the differences among the three molecules become further accentuated, and the gaps in the DOS become more prominent. Specifically, in 2TU, the gaps occur around 24 and 26 eV; in 4TU, a gap occurs around 26 eV; and in 2,4dTU, a pronounced gap emerges at 22 eV with an additional smaller gap near 26 eV. Figure S2 in the supplementary material compares the DOS from the EOM-DIP-CCSD($2h$) and EOM-DIP-CCSD($2h, 3h1p$) calculations, with energies from the former shifted to match the onset. Despite these differences between the two approaches due to correlation, the shapes of the DOS are qualitatively similar.

## C. Auger spectra computed with Koopmans-based approach

### 1. Carbon edge

The C K-edge Auger spectra of the thionated uracils include contributions from the four carbon atoms. Figure S3 in the supplementary material and Fig. 8 show the experimental spectra and the spectra computed within the Koopmans approximation. Two different schemes were employed to determine the spectral intensities. In the first approach (Fig. S3), all decay channels were assigned equal weights, effectively resulting in a shifted DOS spectrum. In the second approach, shown in Fig. 8, the intensities were scaled according to Mulliken's populations of carbon atoms in each MO. The two spectra are similar, which is not surprising, given that nearly all valence MOs have significant electron density on the carbon atoms, as evident from Mulliken's population data provided in Tables S1–S3 in the supplementary material.

Comparing with the experiment, we see that the Koopmans-based spectra reproduce the overall shape and energy range of the experimental C K-edge Auger spectra upon a uniform redshift of 18 eV. The experimental spectra extend from ~210 to 275 eV, which is well captured by the calculations. The C K-edge Auger spectra are very dense and exhibit almost no structure. The broad and unstructured shape of the spectra can be attributed to the fact that nearly all decay states have significant electron density on the carbon atoms, leading to Auger transitions with comparable probabilities and, consequently, a DOS-like spectral band.

### 2. Nitrogen edge

We next examine the N K-edge Auger spectra, arising from the decay following core ionization at the two nitrogens. The experimental spectra span ~325–395 eV and, similarly to the C K-edge, are broad, dense, and unstructured. Our theoretical spectra constructed using either equal weights (Fig. S4 in the supplementary material) or Mulliken's weights (Fig. 9) agree well with the experiment upon a uniform shift of 22 eV. The theoretical spectra largely resemble the DOS, reflecting the fact that most MOs have substantial Mulliken populations on the nitrogens. The band maximum observed between 365 and 375 eV arises due to a high density of decay states in this region. We note that the Mulliken-weighted spectra better capture the lower Auger energy region, where the equal-weight spectra (Fig. S4) tend to overestimate the intensities compared to the experiment, particularly for 2,4dTU.

### 3. Oxygen edge

In contrast to the C and N K-edges, the O K-edge Auger spectra are more structured, and their shapes differ from the DOS. In both 2TU and 4TU, the spectra show two bands—a more intense one between 495 and 510 eV and a less intense one between 470 and 480 eV. Hence, the Koopmans-based spectra with uniform intensities fail to reproduce these features, as Fig. S5 in the supplementary material illustrates. However, when the intensities are scaled according to Mulliken's populations of the valence MOs, as shown in Fig. 10, the computed spectra qualitatively capture the shape of the experimental spectra. Mulliken's populations reported in Tables S1 and S2 in the supplementary material provide a rationale for these observations.

For 2TU, in the 510–495 eV range, the O K-edge Auger spectra comprise ~100 decay states, predominantly originating from transitions involving the combination of outer–mid, outer–inner, and mid–mid valence molecular orbitals. The major contributions arise from orbitals with substantial Mulliken's populations on the oxygen atom, including the outer-valence orbitals $5a''$, $26a'$, and $3a''$ as well as the mid-valence orbitals $22a'$ and $24a'$. The high density of states, along with the presence of combinations of outer-mid MOs that have significant electron density on the O atom, results

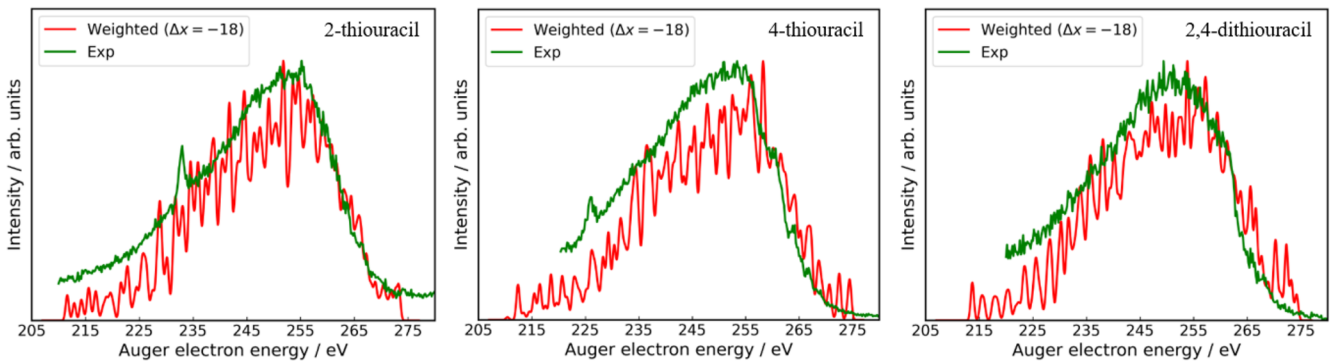


**FIG. 8.** Thiouracils: The C K-edge Auger spectra computed within the Koopmans framework with intensities based on Mulliken's populations.

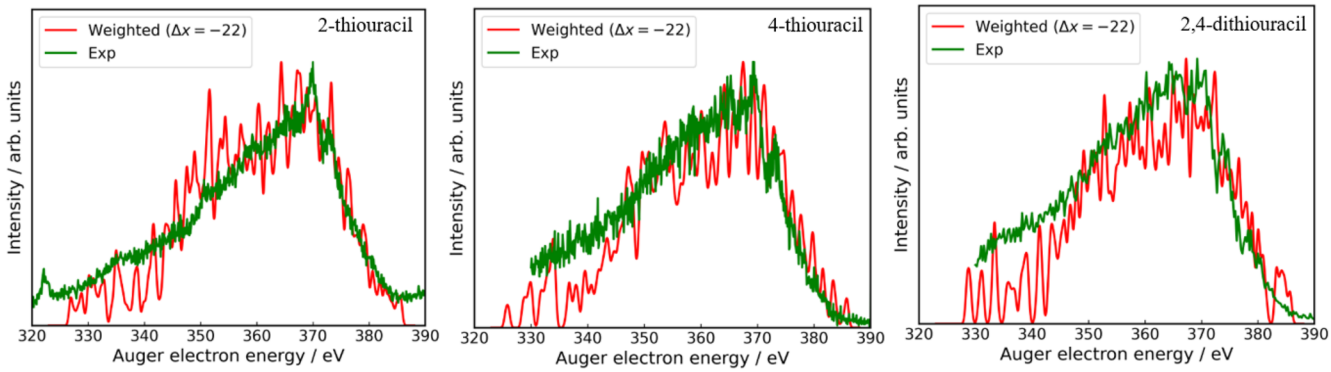


**FIG. 9.** Thiouracils: The N K-edge Auger spectra computed within the Koopmans framework with intensities based on Mulliken's populations.

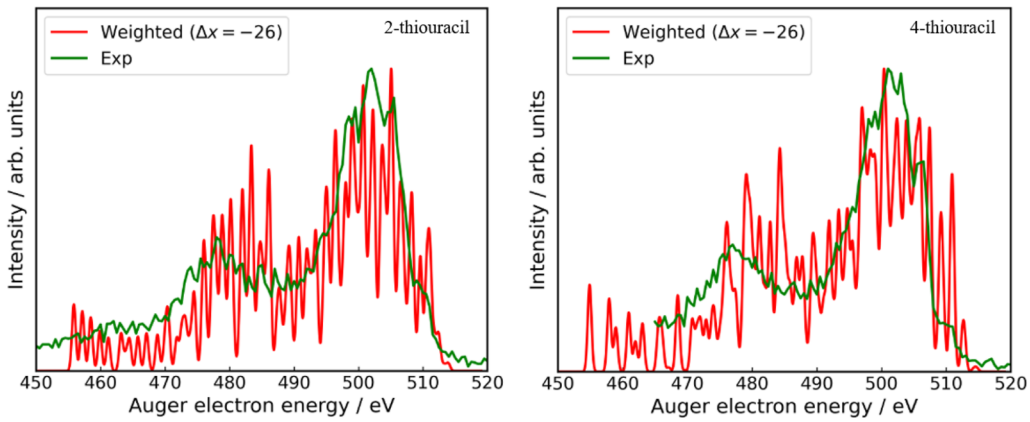


**FIG. 10.** Thiouracils: The O K-edge Auger spectra computed within the Koopmans framework with intensities based on Mulliken's populations.

in the intense band in that range. Between 495 and 480 eV, the spectra include roughly 70 decay states, primarily associated with outer–inner and mid–inner valence transitions. These states are dominated by inner-valence orbitals, with negligible involvement from the HOMO through HOMO-3. The peaks in this region mainly originate from orbitals with large density on oxygen—such as $22a'$, $24a'$, and $3a''$—resulting in the dip in intensity. In the lower energy range (480–470 eV), there are about 15 decay states, arising predominantly from mid–inner and inner–inner valence combinations. No significant contributions from outer-valence orbitals are observed here. We assign the second, less intense band around 470–480 eV to the oxygen-rich orbitals, including $12a'$, $13a'$, $22a'$, and $24a'$. A similar trend is observed in 4TU. The distinct two-band spectral shape and better-resolved peaks arise because, in contrast to the C or N K-edges, only a few valence MOs show significant electron density on the oxygen atoms. We note that a similar two-band structure observed in the O K-edge Auger spectrum of carbon monoxide was explained using similar MO-based arguments.[76]

It is well documented that Mulliken's populations are sensitive to the basis set, which may lead to artifacts in interpretation.[90] To address this issue, we computed the O K-edge spectra using two basis sets; the results are shown in Fig. S6 in the supplementary material. While the individual orbital Mulliken's populations do differ between the basis sets, the computed spectra are very similar, which can be attributed to the high DOS of the decay states.

### 4. Sulfur edge

The S $L_{2,3}$ edge, which originates from the ionization of the S($2p$) orbitals, yields the most structured experimental spectra. Figures 11 and S7 in the supplementary material compare Koopmans-based Auger spectra computed with Mulliken's populations and with equal weights for each decay channel, respectively. As anticipated, the DOS-like spectrum fails to reproduce the experimental structure because, similarly to the O K-edge, only a limited subset of MOs have substantial electron density on sulfur. For 2TU, the outer-valence MOs ($6a''$, $27a'$, $5a''$, and $25a'$) have large Mulliken's populations on S, whereas the mid- and inner-valence MOs have very low weights on S. Consequently, the S L-edge Auger spectrum is dominated by a few intense features concentrated in a relatively narrow energy range.

The Mulliken-weighted Koopmans spectra in Fig. 11 differ considerably from the experimental spectra. Whereas the O K-edge Mulliken-weighted spectra qualitatively reproduce the experimental trends, the agreement degrades at the S $L_{2,3}$ edge. This can be

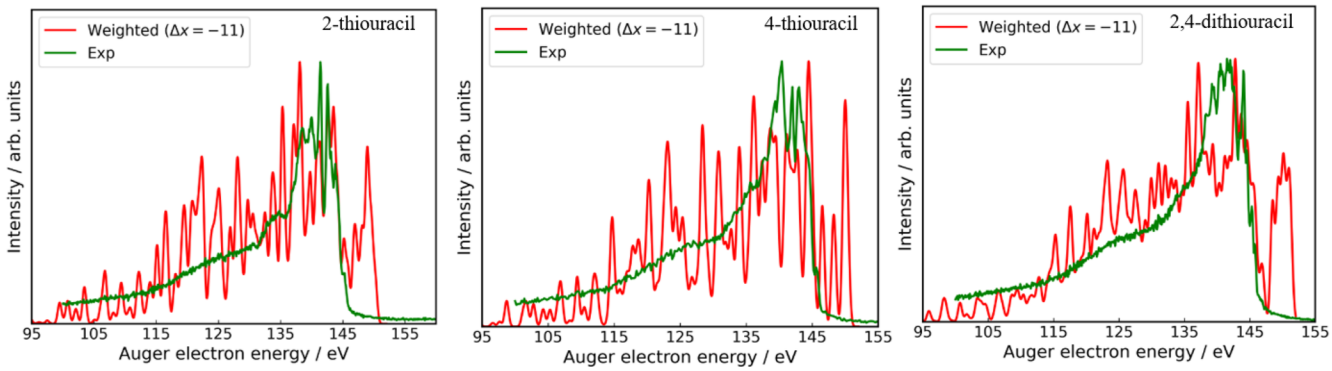


**FIG. 11.** Thiouracils: The S $L_{2,3}$-edge Auger spectra computed within the Koopmans framework with intensities based on Mulliken's populations.

attributed to the sensitivity of Auger decay to the alignment of the initial core-ionized state and the final doubly ionized states, as we had observed[57] for the $L_{2,3}$ edge in $H_2S$. Because the $S(2p)$ core orbitals are directional, their overlap with valence MOs depends on orientation; such effects are absent at the K-edge owing to the spherical shapes of $1s$ orbitals. Consequently, Mulliken-weighted Koopmans spectra are of limited utility for the $L_{2,3}$ edge. For example, there are high intensity peaks in the higher Auger electron energy range that are absent in the experimental spectra, a consequence of neglecting the effects of relative orbital orientations in the initial and final states in Auger decay. Hence, in order to analyze the spectra at the $L_{2,3}$-edge more rigorously, explicit calculation of partial widths becomes necessary.

### D. The effect of correlation on the decay widths: Nitrogen and oxygen edges

We next compute the partial decay widths using the FF approach. Since the Koopmans-based Auger spectra already provide a satisfactory description for the C K-edge, we focus our discussion on the N and O K-edges. For these edges, we construct the $2h$ states using three levels of theory: EOM-DIP-CCSD$(2h)$, EOM-DIP-CCSD$(2h)$ with a perturbative account of the $3h1p$ determinants, and full EOM-DIP-CCSD. The resulting Auger spectra exhibit noticeable differences depending on the level of correlation used for the DIP states. In particular, even a single $(2h, 3h1p)$ iteration on top of EOM-DIP-CCSD$(2h)$ leads to pronounced changes in the computed partial widths.

Figure 12 shows the N K-edge Auger spectra computed using the intermediate DIP FF-PW approach. The corresponding spectra obtained with EOM-DIP-CCSD$(2h)$ and full EOM-DIP-CCSD are shown in Figs. S8 and S9, respectively. With the intermediate DIP FF-PW approach, we were able to span an energy window of about 30 eV. Although the agreement with the experiment is far from perfect, the computed spectra capture the main features. In particular, for 4TU and 2,4dTU, we observe weaker peaks at higher Auger electron energies, followed by intense peaks that reproduce the overall pattern seen in the experimental spectra. When we move to full EOM-DIP-CCSD (Fig. S9), the agreement between theory and experiment improves; however, these calculations are restricted to a narrower energy range of roughly 12 eV, which limits the scope of quantitative comparison. As expected, the dominant peaks in this window originate from $2h$ states formed predominantly from outer-valence MOs.

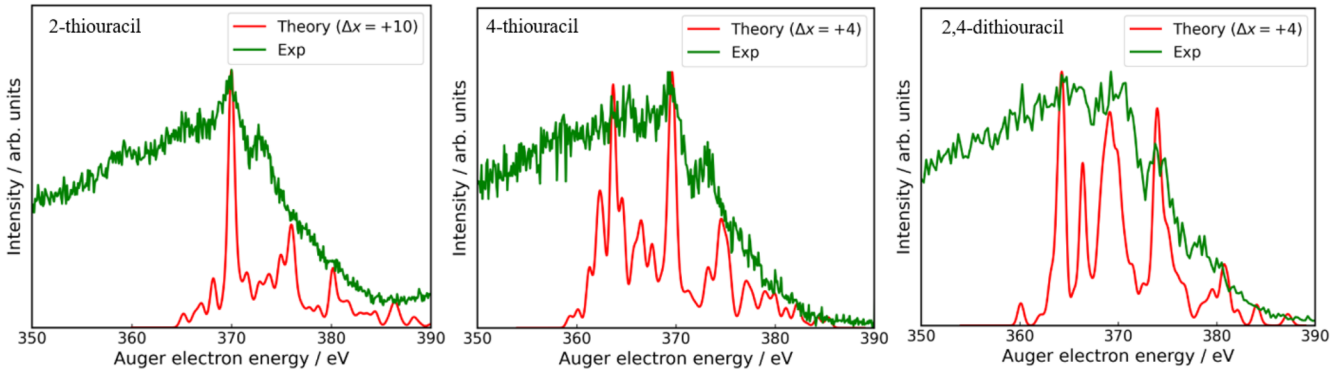


**FIG. 12.** Thiouracils: The N K-edge Auger spectra computed using the FF-PW approach with decay states calculated using EOM-DIP-CCSD$(2h)$ with a single iteration including $3h1p$ determinants.

At the O K-edge, the impact of correlation becomes even more pronounced. For both 2TU and 4TU, the Auger spectra computed at the intermediate correlation level reproduce the main spectral features, as shown in Fig. 13. The peaks at energies around ≥510 eV arise almost exclusively from double ionizations involving the HOMO and HOMO-1; their relatively low intensity is consistent with small Mulliken's populations on the O atom for these orbitals. In contrast, the intense peaks near 500 eV originate from decay channels involving the $5a''$, $27a'$ MOs, which carry larger Mulliken's populations on O. The computed spectra also exhibit a decrease in intensity below 500 eV, in line with the experiment. This trend is absent in the EOM-DIP-CCSD($2h$) spectra for 4TU in Fig. S10, highlighting a redistribution of intensity as the level of correlation is increased. Unfortunately, our calculations do not span the full experimental energy range and, therefore, cannot describe the rise in intensity observed around 480 eV. In contrast, the Koopmans spectra in Fig. 10 capture this feature quite well. The FF-PW spectra obtained with full EOM-DIP-CCSD provide an even more accurate description, but, as in the N K-edge case, they are restricted to a relatively narrow energy window of about 12 eV, as shown in Fig. S11.

These results highlight the importance of the correlation treatment in calculations of Auger decay rates. For quantitative accuracy, it is desirable to use full EOM-DIP-CCSD to describe the decay channels. However, an approximate treatment, EOM-DIP-CCSD($2h$) with a perturbative account of $3h1p$ determinants, provides a reasonable compromise. Our results highlight the need to develop new algorithms for EOM-CCSD calculations when many target states are needed.

### E. Sulfur $L_{2,3}$-edge

From a theoretical perspective, the S $L_{2,3}$-edge is the most intriguing, as its treatment must account not only for correlation effects but also for relativistic effects. In sulfur, the relativistic effects are dominated by SOC, which mixes the $2p$ orbitals and splits them into the $2p_{1/2}$ and $2p_{3/2}$ components. The impact of SOC is clearly visible in the S $L_{2,3}$-edge XPS spectra of the thiouracils shown in Fig. S12. For all three molecules, the non-relativistic spectra exhibit a single peak: the three $2p$ orbitals are split only slightly by the molecular field. Upon inclusion of SOC, the single peak splits into two distinct features with an approximate 2:1 intensity ratio,

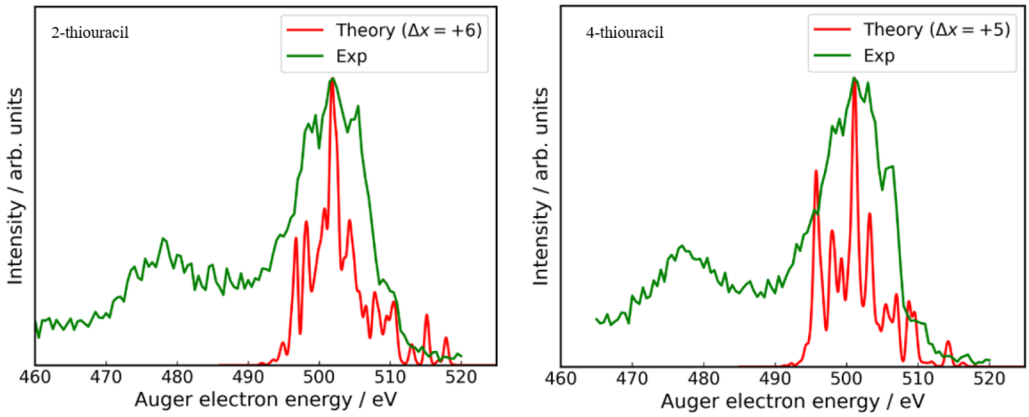


**FIG. 13.** Thiouracils: The O K-edge Auger spectra computed using the FF-PW approach with decay states calculated using EOM-DIP-CCSD($2h$) with a single iteration including $3h1p$ determinants.

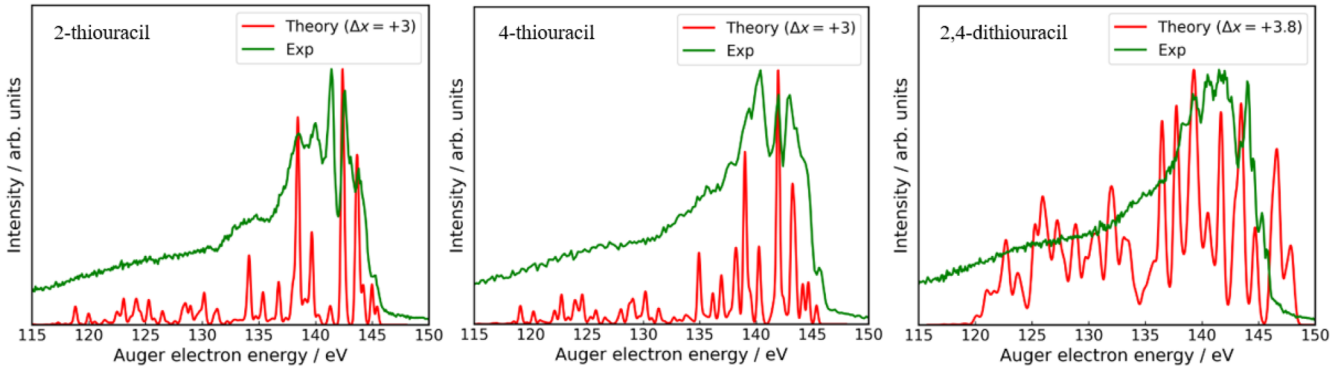


**FIG. 14.** Thiouracils: The S $L_{2,3}$-edge Auger spectra computed using the FF-CW approach with decay states calculated using EOM-DIP-CCSD($2h$) with a single iteration including $3h1p$ determinants.

corresponding to the $L_2$ and $L_3$ edges. The resulting SOC splitting of about 1.2 eV for the thiouracils is in good agreement with a previous study.[73]

In what follows, we focus on the relativistic calculations. The S $L_{2,3}$-edge Auger spectra are the most structured among all edges, with intense features concentrated between 135 and 150 eV, as shown in Fig. 14. Below 135 eV, the intensity gradually decreases. This behavior can be rationalized by the fact that the relative orientation between the core-ionized and decay states is important in Auger decay. Therefore, only decay states that overlap well with the initial core-ionized state yield large Auger intensity. We also find that the spectra computed using approximate EOM-DIP-CCSD 2*h* states reproduce the main experimental features much better than the Koopmans-based spectra constructed from Mulliken's populations given in Fig. 11. For instance, the intensities of the peaks at energies ≥142 eV and ≤135 eV are overestimated in the Koopmans approach, whereas the FF-CW calculations preserve the overall spectral shape well.

The experimental Auger spectrum of 2TU exhibits six well-resolved peaks between 136 and 147 eV. The corresponding theoretical spectrum shows about seven peaks in this energy range. Although the relative intensities of the theoretical peaks are not perfect, the overall spectral shape agrees reasonably well with experiment, with the main exception of the intense experimental peak at 137 eV. For 4TU, there are roughly seven peaks in this energy window and, after applying an energy shift, the theoretical spectra reproduce both the positions and intensities of the experimental features quite well, except for the experimental peak near 142 eV that is absent in the calculations. In contrast, the experimental spectrum of 2,4dTU is less resolved than those of the other two molecules. In our theoretical treatment, we include contributions from both S atoms; the resulting spectra are in qualitative agreement with experiment, although the theoretical intensities deviate more from the experiment compared to 2TU and 4TU.

Next, we analyze the decay channels computed using full EOM-DIP-CCSD. Unlike other edges, our calculated decay states for the S $L_{2,3}$-edge were able to describe the most structured portion of the experimental spectra between 135 and 150 eV, shown in Fig. 15. The increased level of detail in this region allows us to resolve finer features, such as the energy gaps present in the experimental spectra. For example, in the 2TU Auger spectrum, there is a pronounced gap near 142.5 eV, whereas in 4TU a similar gap appears around 141 eV. In 2,4dTU, there is also a gap, but it is less prominent. These gaps are also evident in the theoretical spectra, which are shifted in accordance with the experimental energy gaps.

Figures 15, 16, and S13 in the supplementary material compare the $L_{2,3}$-edge Auger spectra computed using the FF-CW and CBF approaches and the experiment. In contrast to the K-edge Auger spectrum of benzene,[55] the two theoretical approaches do not agree with each other, indicating an increased sensitivity of $L_{2,3}$-edge Auger decay to the treatment of the continuum.

More importantly, although both approaches capture certain experimental features, their overall agreement with the experiment is less satisfactory compared to the $L_{2,3}$-edge Auger spectrum of $H_2S$.[57] For all three molecules, the CBF approach provides a better description of the higher-energy region; for example, in the cases of 4TU and 2,4dTU, CBF reproduces peak intensities that are comparable to the experiment. However, as we move toward lower Auger electron energies, the FF-CW approach yields improved agreement, capturing the spectral features more accurately than CBF in this region.

These observations underscore the need for further methodological developments in modeling $L_{2,3}$-edge Auger decay. Within the FF framework, this highlights the importance of developing an *ab initio* description of the continuum electron, beyond simplistic models such as PW or CW. For the CBF approach, greater attention must be given to the design and optimization of complex functions, as their spatial extent and scaling parameters critically affect the description of the outgoing electron. In this context, systematically converging the basis and assessing its transferability across different edges is essential.

Finally, these findings motivate the exploration of approximate yet efficient frameworks, such as OCA,[49] particularly for $L_{2,3}$-edge Auger decay. Benchmarking OCA performance and comparing it with FF and CBF approaches may provide valuable insight into the balance between computational efficiency and accuracy and help identify the key physical ingredients required for reliable modeling of L-edge Auger spectra.

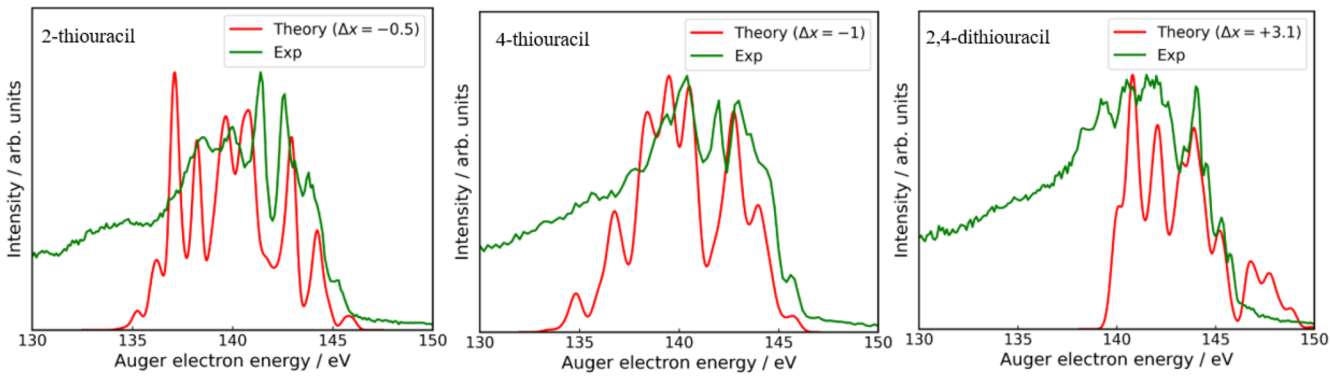


**FIG. 15.** Thiouracils: The S $L_{2,3}$ edge Auger spectra computed using the FF-CW approach with decay states calculated using full EOM-DIP-CCSD. Gaussian convolution with FWHM = 0.50 eV was used.

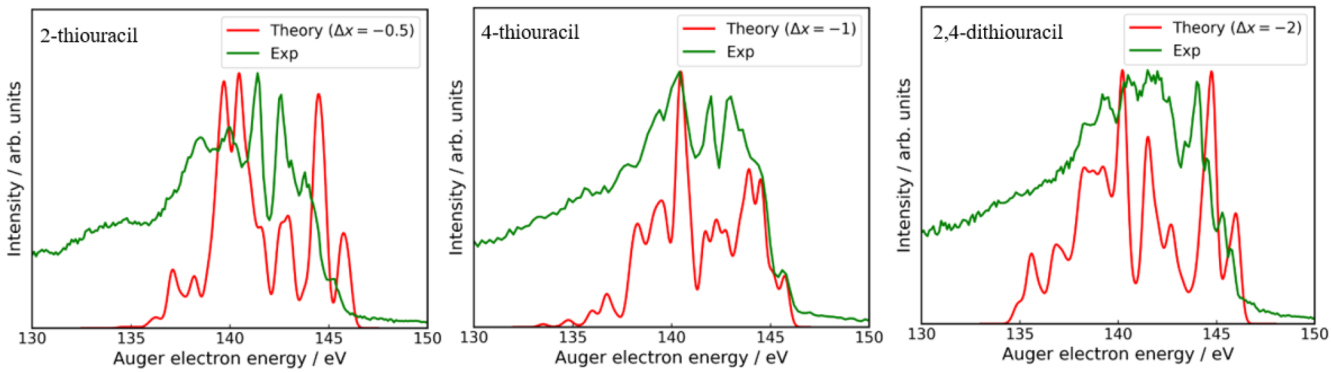


**FIG. 16.** Thiouracils: The S $L_{2,3}$ edge Auger spectra computed using the CBF approach with decay states calculated using full EOM-DIP-CCSD. Gaussian convolution with FWHM = 0.50 eV was used.

## V. CONCLUSION

We have presented a comprehensive study of the Auger spectra in three thionated uracils (Fig. 1), comparing theoretical results with the experimental spectra. We considered four edges—carbon, nitrogen, and oxygen K-edges (i.e., decay of 1*s* vacancies) and the sulfur $L_{2,3}$ edge (i.e., decay of 2*p* vacancies). Even though the decay channels (valence 2*h* states) are the same for all edges, the resulting Auger spectra are strikingly different, highlighting the local nature of Auger decay. The analysis of the decay states in terms of Mulliken's populations provides an explanation: the spectra are broad and featureless for carbon and nitrogen edges because nearly all valence MOs have large weights on these atoms, but structure emerges for the oxygen and sulfur edges because only a few MOs have large weights on these atoms.

The dense spectra of the C, N, and O edges can be well described by the Koopmans approximation combined with Mulliken's populations. However, finer details require correlated treatments. The sulfur edge spectra show much more structure, revealing interesting differences among the three molecules. Quantitative description of these spectra has proven to be challenging, as it requires a high-level of electron correlation, the inclusion of spin–orbit interactions, and an accurate treatment of the continuum.

The S $L_{2,3}$-edge Auger spectra highlight the increased complexity of modeling L-edge decay, where both SOC and continuum-electron effects play a critical role. While correlated EOM-DIP-CCSD descriptions capture the overall spectral structure and key experimental features, noticeable discrepancies in intensities and peak positions remain. In particular, the differences between the FF-CW and CBF results, along with their relatively poor agreement with the experiment, underscore the higher sensitivity of $L_{2,3}$-edge spectra to the treatment of the continuum electron. These findings point to limitations of current approaches and emphasize the need for improved methodologies, including *ab initio* continuum descriptions within the FF framework, better-optimized complex exponents in the CBF approach, and systematic benchmarking of approximate schemes such as the OCA.

We conclude by emphasizing the crucial role of the synergy between theory and experiment in advancing our understanding of complex x-ray-induced phenomena such as Auger decay in polyatomic molecules.

## SUPPLEMENTARY MATERIAL

The supplementary material encompasses relevant Cartesian geometries, basis sets, input details, additional results, spectra, and information about *Zenodo* deposition.

## ACKNOWLEDGMENTS

This study was supported in Los Angeles by the U.S. National Science Foundation (Grant No. CHE-2525964 to A.I.K.). The experimental spectra were recorded at the PLEIADES beamline at the synchrotron SOLEIL, France, under proposal Grant Nos. 20200549 and 20211636. We acknowledge SOLEIL for the provision of synchrotron radiation facilities and E. Robert and C. Nicolas for their technical help during the beamtime at PLEIADES. We are grateful to the Volkswagen Foundation for funding via a Lichtenberg Professorship, to BMBF for funding via Verbundforschungsprojekt Grant No. 05K19IP1, and to DFG for funding via Grant No. GU 1478/1-1.

## AUTHOR DECLARATIONS

### Conflict of Interest

The authors declare the following competing financial interests: A.I.K. is the president and a part-owner of Q-Chem, Inc.

### Author Contributions

N.K.J. and D.M. contributed equally to this study.

**Nayanthara K. Jayadev**: Conceptualization (equal); Formal analysis (equal); Investigation (lead); Software (lead); Validation (equal); Visualization (lead); Writing – original draft (equal); Writing – review & editing (equal). **Dennis Mayer**: Conceptualization (equal); Investigation (equal); Methodology (equal); Writing – original draft

(supporting); Writing – review & editing (equal). **Florian Matz**: Investigation (supporting); Methodology (equal); Software (equal). **Fabiano Lever**: Investigation (supporting); Methodology (supporting). **Lisa Mehner**: Investigation (supporting). **Constantin Walz**: Investigation (supporting). **Marta L. Murillo-Sánchez**: Investigation (supporting). **John Bozek**: Investigation (supporting). **Thomas-C. Jagau**: Conceptualization (equal); Formal analysis (equal); Methodology (equal); Project administration (supporting); Supervision (supporting); Writing – review & editing (equal). **Markus Gühr**: Conceptualization (lead); Formal analysis (equal); Funding acquisition (lead); Investigation (equal); Methodology (equal); Project administration (lead); Supervision (lead); Validation (equal); Writing – original draft (equal); Writing – review & editing (equal). **Anna I. Krylov**: Conceptualization (lead); Funding acquisition (lead); Investigation (lead); Methodology (equal); Project administration (lead); Resources (equal); Software (equal); Supervision (lead); Writing – original draft (equal); Writing – review & editing (equal).

## DATA AVAILABILITY

The data that support the findings of this study are available within the article, the associated supplementary material, and the *Zenodo* deposition.

## REFERENCES


[1] L. S. Cederbaum, W. Domcke, and J. Schirmer, "Many-body theory of core holes," Phys. Rev. A **22**, 206 (1980).

[2] R. J. Bartlett and I. Shavitt, *Many-Body Methods in Chemistry and Physics: MBPT and Coupled-Cluster Theory*, *Cambridge Molecular Science* (Cambridge University Press, 2009), pp. 1–532, ISBN: 978-0-511-59683-4.

[3] A. I. Krylov, "Equation-of-motion coupled-cluster methods for open-shell and electronically excited species: The hitchhiker's guide to Fock space," Annu. Rev. Phys. Chem. **59**, 433 (2008).

[4] R. J. Bartlett, "Coupled-cluster theory and its equation-of-motion extensions," WIREs: Comput. Mol. Sci. **2**, 126 (2012).

[5] S. Coriani and H. Koch, "Communication: X-ray absorption spectra and core-ionization potentials within a core-valence separated coupled cluster framework," J. Chem. Phys. **143**, 181103 (2015).

[6] S. Coriani and H. Koch, "Erratum: 'Communication: X-ray absorption spectra and core-ionization potentials within a core-valence separated coupled cluster framework [J. Chem. Phys. 143, 181103 (2015)]'" J. Chem. Phys. **145**, 149901 (2016).

[7] M. L. Vidal, X. Feng, E. Epifanovsky, A. I. Krylov, and S. Coriani, "A new and efficient equation-of-motion coupled-cluster framework for core-excited and core-ionized states," J. Chem. Theory Comput. **15**, 3117 (2019).

[8] M. L. Vidal, A. I. Krylov, and S. Coriani, "Dyson orbitals within the fc-CVS-EOM-CCSD framework: Theory and application to X-ray photoelectron spectroscopy of ground and excited states," Phys. Chem. Chem. Phys. **22**, 2693 (2020).

[9] M. L. Vidal, A. I. Krylov, and S. Coriani, "Correction to: 'Dyson orbitals within the fc-CVS-EOM-CCSD framework: Theory and application to X-ray photoelectron spectroscopy of ground and excited states,'" Phys. Chem. Chem. Phys. **22**, 3744 (2020).

[10] K. D. Nanda, M. L. Vidal, R. Faber, S. Coriani, and A. I. Krylov, "How to stay out of trouble in RIXS calculations within the equation-of-motion coupled-cluster damped response theory? Safe hitchhiking in the excitation manifold by means of core-valence separation," Phys. Chem. Chem. Phys. **22**, 2629 (2020).

[11] K. D. Nanda, M. L. Vidal, R. Faber, S. Coriani, and A. I. Krylov, "Correction: 'how to stay out of trouble in RIXS calculations within the equation-of-motion coupled-cluster damped response theory? Safe hitchhiking in the excitation manifold by means of core-valence separation,'" Phys. Chem. Chem. Phys. **22**, 17749 (2020).

[12] R. Faber and S. Coriani, "Resonant inelastic X-ray scattering and nonresonant X-ray emission spectra from coupled-cluster (damped) response theory," J. Chem. Theory Comput. **15**, 520 (2019).

[13] R. Faber and S. Coriani, "Core–valence-separated coupled-cluster-singles-and-doubles complex-polarization-propagator approach to X-ray spectroscopies," Phys. Chem. Chem. Phys. **22**, 2642 (2020).

[14] M. L. Vidal, M. Epshtein, V. Scutelnic, Z. Yang, T. Xue, S. R. Leone, A. I. Krylov, and S. Coriani, "The interplay of open-shell spin-coupling and Jahn–Teller distortion in benzene radical cation probed by x-ray spectroscopy," J. Phys. Chem. A **124**, 9532 (2020).

[15] S. L. Sorensen, X. Zheng, S. H. Southworth, M. Patanen, E. Kokkonen, B. Oostenrijk, O. Travnikova, T. Marchenko, M. Simon, C. Bostedt *et al.*, "From synchrotrons for XFELs: The soft x-ray near-edge spectrum of the ESCA molecule," J. Phys. B: At., Mol. Opt. Phys. **53**, 244011 (2020).

[16] F. Tarantelli, A. Sgamellotti, L. S. Cederbaum, and J. Schirmer, "Theoretical investigation of many dicationic states and the Auger spectrum of benzene," J. Chem. Phys. **86**, 2201 (1987).

[17] E. M.-L. Ohrendorff, F. Tarantelli, and L. S. Cederbaum, "Dicationic states of hydrocarbons and a statistical approach to their Auger spectra," J. Chem. Phys. **92**, 2984 (1990).

[18] N. Moiseyev, *Non-Hermitian Quantum Mechanics* (Cambridge University Press, 2011).

[19] F. Matz and T.-C. Jagau, "Channel-specific core-valence projectors for determining partial Auger decay widths," Mol. Phys. **121**, e2105270 (2022).

[20] F. Matz and T.-C. Jagau, "Molecular Auger decay rates from complex-variable coupled-cluster theory," J. Chem. Phys. **156**, 114117 (2022).

[21] V. Carravetta and H. Ågren, "Stieltjes imaging method for molecular Auger transition rates: Application to the Auger spectrum of water," Phys. Rev. A **35**, 1022 (1987).

[22] V. Averbukh and L. S. Cederbaum, "*Ab initio* calculation of interatomic decay rates by a combination of the Fano ansatz, Green's-function methods, and the Stieltjes imaging technique," J. Chem. Phys. **123**, 204107 (2005).

[23] S. Kopelke, K. Gokhberg, L. S. Cederbaum, F. Tarantelli, and V. Averbukh, "Autoionization widths by Stieltjes imaging applied to Lanczos pseudospectra," J. Chem. Phys. **134**, 024106 (2011).

[24] E. J. McGuire, "*K*-shell Auger transition rates and fluorescence yields for elements Be–Ar," Phys. Rev. **185**, 1 (1969).

[25] H. Ågren, S. Svensson, and U. I. Wahlgren, "SCF and limited CI calculations for assignment of the Auger spectrum and of the satellites in the soft x-ray spectrum of $H_2O$," Chem. Phys. Lett. **35**, 336 (1975).

[26] R. Manne and H. Ågren, "Auger transition amplitudes from general many-electron wavefunctions," Chem. Phys. **93**, 201 (1985).

[27] F. Tarantelli, A. Sgamellotti, and L. S. Cederbaum, "The calculation of molecular Auger spectra," J. Electron Spectrosc. Relat. Phenom. **68**, 297 (1994).

[28] H. Siegbahn, L. Asplund, and P. Kelfve, "The Auger electron spectrum of water vapour," Chem. Phys. Lett. **35**, 330 (1975).

[29] H. Ågren, "On the interpretation of molecular valence Auger spectra," J. Chem. Phys. **75**, 1267 (1981).

[30] E. Z. Chelkowska and F. P. Larkins, "Auger spectroscopy for molecules: Tables of matrix elements for transition-rate calculations corresponding to an *s*-, *p*-, or *d*-type initial hole," At. Data Nucl. Data Tables **49**, 121 (1991).

[31] K. Zähringer, H.-D. Meyer, and L. S. Cederbaum, "Molecular scattering wave functions for Auger decay rates: The Auger spectrum of hydrogen fluoride," Phys. Rev. A **45**, 318 (1992).

[32] R. F. Fink, M. N. Piancastelli, A. N. Grum-Grzhimailo, and K. Ueda, "Angular distribution of Auger electrons from fixed-in-space and rotating C $1s \rightarrow 2\pi$ photoexcited CO: Theory," J. Chem. Phys. **130**, 014306 (2009).

[33] G. Grell, O. Kühn, and S. I. Bokarev, "Multireference quantum chemistry protocol for simulating autoionization spectra: Test of ionization continuum models for the neon atom," Phys. Rev. A **100**, 042512 (2019).

[34] G. Grell and S. I. Bokarev, "Multi-reference protocol for (auto) ionization spectra: Application to molecules," J. Chem. Phys. **152**, 074108 (2020).

[35]L. Inhester, C. F. Burmeister, G. Groenhof, and H. Grubmüller, "Auger spectrum of a water molecule after single and double core ionization," J. Chem. Phys. **136**, 144304 (2012).
[36]P. Kolorenč and V. Averbukh, "Fano-ADC(2,2) method for electronic decay rates," J. Chem. Phys. **152**, 214107 (2020).
[37]R. R. Rye, T. E. Madey, J. E. Houston, and P. H. Holloway, "Chemical-state effects in Auger electron spectroscopy," J. Chem. Phys. **69**, 1504 (1978).
[38]R. R. Rye, D. R. Jennison, and J. E. Houston, "Auger spectra of alkanes," J. Chem. Phys. **73**, 4867 (1980).
[39]R. R. Rye and J. E. Houston, "Molecular Auger spectroscopy," Acc. Chem. Res. **17**, 41 (1984).
[40]R. Fink, "Theoretical autoionization spectra of $1s \rightarrow \pi^*$ excited $N_2$ and $N_2O$," J. Electron Spectrosc. Relat. Phenom. **76**, 295 (1995).
[41]R. F. Fink, M. Kivilompolo, H. Aksela, and S. Aksela, "Spin-orbit interaction and molecular-field effects in the $L_{2,3}VV$ Auger-electron spectra of HCl," Phys. Rev. A **58**, 1988 (1998).
[42]S.-K. Son, L. Young, and R. Santra, "Impact of hollow-atom formation on coherent x-ray scattering at high intensity," Phys. Rev. A **83**, 033402 (2011).
[43]V. Sekushin, R. Püttner, R. F. Fink, M. Martins, Y. H. Jiang, H. Aksela, S. Aksela, and G. Kaindl, "A comprehensive study of the vibrationally resolved S $2p^{-1}$ Auger electron spectrum of carbonyl sulfide," J. Chem. Phys. **137**, 044310 (2012).
[44]L. Inhester, K. Hanasaki, Y. Hao, S.-K. Son, and R. Santra, "X-ray multiphoton ionization dynamics of a water molecule irradiated by an x-ray free-electron laser pulse," Phys. Rev. A **94**, 023422 (2016).
[45]B. N. C. Tenorio, T. A. Voß, S. I. Bokarev, P. Decleva, and S. Coriani, "Multireference approach to normal and resonant Auger spectra based on the one-center approximation," J. Chem. Theory Comput. **18**, 4387 (2022).
[46]W. Skomorowski and A. I. Krylov, "Feshbach–Fano approach for calculation of Auger decay rates using equation-of-motion coupled-cluster wave functions. I. Theory and implementation," J. Chem. Phys. **154**, 084124 (2021).
[47]W. Skomorowski and A. I. Krylov, "Feshbach–Fano approach for calculation of Auger decay rates using equation-of-motion coupled-cluster wave functions. II. Numerical examples and benchmarks," J. Chem. Phys. **154**, 084125 (2021).
[48]N. K. Jayadev, W. Skomorowski, and A. I. Krylov, "Molecular-orbital framework of two-electron processes: Application to Auger and intermolecular Coulomb decay," J. Phys. Chem. Lett. **14**, 8612 (2023).
[49]W. Skomorowski, B. N. C. Tenorio, and S. Coriani, "An equation-of-motion coupled cluster singles and doubles approach to Auger–Meitner spectra based on the one-center approximation," Phys. Chem. Chem. Phys. **27**, 20117 (2025).
[50]T. N. Rescigno, C. W. McCurdy, and A. E. Orel, "Extensions of the complex-coordinate method to the study of resonances in many-electron systems," Phys. Rev. A **17**, 1931 (1978).
[51]A. F. White, M. Head-Gordon, and C. W. McCurdy, "Complex basis functions revisited: Implementation with applications to carbon tetrafluoride and aromatic N-containing heterocycles within the static-exchange approximation," J. Chem. Phys. **142**, 054103 (2015).
[52]F. Matz, A. Gkogkos, and T.-C. Jagau, "Computation of partial Auger decay widths from complex-valued equation-of-motion coupled-cluster energies," J. Phys. Chem. A **130**, 2252 (2026).
[53]G. Wentzel, "Über strahlungslose quantensprünge," Z. Physik **43**, 524 (1927).
[54]F. Matz, J. Nijssen, and T.-C. Jagau, "Ab initio investigation of the Auger spectra of methane, ethane, ethylene, and acetylene," J. Phys. Chem. A **127**, 6147 (2023).
[55]N. K. Jayadev, A. Ferino-Pérez, F. Matz, A. I. Krylov, and T.-C. Jagau, "The Auger spectrum of benzene," J. Chem. Phys. **158**, 064109 (2023).
[56]N. K. Jayadev, T.-C. Jagau, and A. I. Krylov, "Resonant Auger decay in benzene," J. Phys. Chem. A **129**, 733 (2025).
[57]N. K. Jayadev, W. Skomorowski, and A. I. Krylov, "Incorporating the effect of spin–orbit interaction in Auger decay spectra: Theory and examples," J. Chem. Phys. **163**, 114104 (2025).
[58]P.-Å. Malmqvist and B. O. Roos, "The CASSCF state interaction method," Chem. Phys. Lett. **155**, 189 (1989).
[59]B. O. Roos and P.-Å. Malmqvist, "Relativistic quantum chemistry: The multiconfigurational approach," Phys. Chem. Chem. Phys. **6**, 2919 (2004).
[60]P. Pokhilko, E. Epifanovsky, and A. I. Krylov, "General framework for calculating spin–orbit couplings using spinless one-particle density matrices: Theory and application to the equation-of-motion coupled-cluster wave functions," J. Chem. Phys. **151**, 034106 (2019).
[61]E. Epifanovsky, K. Klein, S. Stopkowicz, J. Gauss, and A. I. Krylov, "Spin–orbit couplings within the equation-of-motion coupled-cluster framework: Theory, implementation, and benchmark calculations," J. Chem. Phys. **143**, 064102 (2015).
[62]M. L. Vidal, P. Pokhilko, A. I. Krylov, and S. Coriani, "Equation-of-motion coupled-cluster theory to model L-edge x-ray absorption and photoelectron spectra," J. Phys. Chem. Lett. **11**, 8314 (2020).
[63]P. Ajitkumar and J. D. Cherayil, "Thionucleosides in transfer ribonucleic acid: Diversity, structure, biosynthesis, and function," Microbiol. Rev. **52**, 103 (1988).
[64]S. Zhang, J. C. Blain, D. Zielinska, S. M. Gryaznov, and J. W. Szostak, "Fast and accurate nonenzymatic copying of an RNA-like synthetic genetic polymer," Proc. Natl. Acad. Sci. U. S. A. **110**, 17732 (2013).
[65]S. Arslancan, L. Martínez-Fernández, and I. Corral, "Photophysics and photochemistry of canonical nucleobases' thioanalogs: From quantum mechanical studies to time resolved experiments," Molecules **22**, 998 (2017).
[66]B. Ashwood, M. Pollum, and C. E. Crespo-Hernández, "Photochemical and photodynamical properties of sulfur-substituted nucleic acid bases," Photochem. Photobiol. **95**, 33 (2019).
[67]K. Kramer, P. Hummel, H.-H. Hsiao, X. Luo, M. Wahl, and H. Urlaub, "Mass-spectrometric analysis of proteins cross-linked to 4-thio-uracil- and 5-bromo-uracil-substituted RNA," Int. J. Mass Spectrom. **304**, 184 (2011).
[68]S. Mai, P. Marquetand, and L. González, "Intersystem crossing pathways in the noncanonical nucleobase 2-thiouracil: A time-dependent picture," J. Phys. Chem. Lett. **7**, 1978 (2016).
[69]S. Mai, M. Pollum, L. Martínez-Fernández, N. Dunn, P. Marquetand, I. Corral, C. E. Crespo-Hernández, and L. González, "The origin of efficient triplet state population in sulfur-substituted nucleobases," Nat. Commun. **7**, 13077 (2016).
[70]F. Lever, D. Mayer, D. Picconi, J. Metje, S. Alisauskas, F. Calegari, S. Düsterer, C. Ehlert, R. Feifel, M. Niebuhr, B. Manschwetus, M. Kuhlmann, T. Mazza, M. S. Robinson, R. J. Squibb, A. Trabattoni, M. Wallner, P. Saalfrank, T. J. A. Wolf, and M. Gühr, "Ultrafast dynamics of 2-thiouracil investigated by time-resolved Auger spectroscopy," J. Phys. B: At., Mol. Opt. Phys. **54**, 014002 (2020).
[71]F. Lever, D. Mayer, J. Metje, S. Alisauskas, F. Calegari, S. Dústerer, R. Feifel, M. Niebuhr, B. Manschwetus, M. Kuhlmann, T. Mazza, M. S. Robinson, R. J. Squibb, A. Trabattoni, M. Wallner, T. J. A. Wolf, and M. Gühr, "Core-level spectroscopy of 2-thiouracil at the sulfur $L_1$- and $L_{2,3}$-edges utilizing a SASE free-electron laser," Molecules **26**, 6469 (2021).
[72]D. Mayer, F. Lever, D. Picconi, J. Metje, S. Alisauskas, F. Calegari, S. Düsterer, C. Ehlert, R. Feifel, M. Niebuhr, B. Manschwetus, M. Kuhlmann, T. Mazza, M. S. Robinson, J. Squibb, A. Trabattoni, M. Wallner, P. Saalfrank, T. J. A. Wolf, and M. Gühr, "Following excited-state chemical shifts in molecular ultrafast x-ray photoelectron spectroscopy," Nat. Commun. **13**, 198 (2022).
[73]D. Mayer, M. Handrich, D. Picconi, F. Lever, L. Mehner, M. L. Murillo-Sánchez, C. Walz, E. Titov, J. Bozek, P. Saalfrank, and M. Gühr, "X-ray photoelectron and NEXAFS spectroscopy of thionated uracils in the gas phase," J. Chem. Phys. **161**, 134301 (2024).
[74]F. Lever, D. Picconi, D. Mayer, S. Ališauskas, F. Calegari, S. Düsterer, R. Feifel, M. Kuhlmann, T. Mazza, J. Metje, M. S. Robinson, R. J. Squibb, A. Trabattoni, M. Ware, P. Saalfrank, T. J. A. Wolf, and M. Gühr, "Direct observation of the $\pi\pi^*$ to $n\pi^*$ transition in 2-thiouracil via time-resolved NEXAFS spectroscopy," J. Phys. Chem. Lett. **16**, 4038 (2025).
[75]T. Jahnke, S. Mai, S. Bhattacharyya, K. Chen, R. Boll, M. E. Castellani, S. Dold, U. Frühling, A. E. Green, M. Ilchen, R. Ingle, G. Kastirke, H. V. S. Lam, F. Lever, D. Mayer, T. Mazza, T. Mullins, Y. Ovcharenko, B. Senfftleben, F. Trinter, A.-T. Noor, S. Usenko, A. S. Venkatachalam, A. Rudenko, D. Rolles, M. Meyer, H. Ibrahim, and M. Gühr, "Direct observation of ultrafast symmetry reduction during internal conversion of 2-thiouracil using Coulomb explosion imaging," Nat. Commun. **16**, 2074 (2025).
[76]W. E. Moddeman, T. A. Carlson, M. O. Krause, B. P. Pullen, W. E. Bull, and G. K. Schweitzer, "Determination of the *K–LL* Auger spectra of $N_2$, $O_2$, CO, NO, $H_2O$, and $CO_2$," J. Chem. Phys. **55**, 2317 (1971).
[77]N. K. Jayadev and A. I. Krylov, "ezAuger" (2025), http://iopenshell.usc.edu/downloads.
[78]A. I. Krylov, "From orbitals to observables and back," J. Chem. Phys. **153**, 080901 (2020).

[79]J. F. Stanton and R. J. Bartlett, "The equation of motion coupled-cluster method. A systematic biorthogonal approach to molecular excitation energies, transition probabilities, and excited state properties," J. Chem. Phys. **98**, 7029 (1993).
[80]C. M. Oana and A. I. Krylov, "Dyson orbitals for ionization from the ground and electronically excited states within equation-of-motion coupled-cluster formalism: Theory, implementation, and examples," J. Chem. Phys. **127**, 234106 (2007).
[81]C. W. McCurdy and T. N. Rescigno, "Extension of the method of complex basis functions to molecular resonances," Phys. Rev. Lett. **41**, 1364 (1978).
[82]T. N. Rescigno, A. E. Orel, and C. W. McCurdy, "Application of complex coordinate SCF techniques to a molecular shape resonance: The $^2\Pi_g$ state of $N_2^-$," J. Chem. Phys. **73**, 6347 (1980).
[83]C. W. McCurdy, T. N. Rescigno, E. R. Davidson, and J. G. Lauderdale, "Applicability of self-consistent field techniques based on the complex coordinate method to metastable electronic states," J. Chem. Phys. **73**, 3268 (1980).
[84]A. F. White, E. Epifanovsky, C. W. McCurdy, and M. Head-Gordon, "Second order Møller–Plesset and coupled cluster singles and doubles methods with complex basis functions for resonances in electron-molecule scattering," J. Chem. Phys. **146**, 234107 (2017).
[85]R. Sarangi, M. L. Vidal, S. Coriani, and A. I. Krylov, "On the basis set selection for calculations of core-level states: Different strategies to balance cost and accuracy," Mol. Phys. **118**, e1769872 (2020).
[86]E. Epifanovsky, A. T. B. Gilbert, X. Feng, J. Lee, Y. Mao, N. Mardirossian, P. Pokhilko, A. F. White, M. P. Coons, A. L. Dempwolff, Z. Gan, D. Hait, P. R. Horn, L. D. Jacobson, I. Kaliman, J. Kussmann, A. W. Lange, K. U. Lao, D. S. Levine, J. Liu, S. C. McKenzie, A. F. Morrison, K. D. Nanda, F. Plasser, D. R. Rehn, M. L. Vidal, Z.-Q. You, Y. Zhu, B. Alam, B. J. Albrecht, A. Aldossary, E. Alguire, J. H. Andersen, V. Athavale, D. Barton, K. Begam, A. Behn, N. Bellonzi, Y. A. Bernard, E. J. Berquist, H. G. A. Burton, A. Carreras, K. Carter-Fenk, R. Chakraborty, A. D. Chien, K. D. Closser, V. Cofer-Shabica, S. Dasgupta, M. de Wergifosse, J. Deng, M. Diedenhofen, H. Do, S. Ehlert, P.-T. Fang, S. Fatehi, Q. Feng, T. Friedhoff, J. Gayvert, Q. Ge, G. Gidofalvi, M. Goldey, J. Gomes, C. E. González-Espinoza, S. Gulania, A. O. Gunina, M. W. D. Hanson-Heine, P. H. P. Harbach, A. Hauser, M. F. Herbst, M. Hernández Vera, M. Hodecker, Z. C. Holden, S. Houck, X. Huang, K. Hui, B. C. Huynh, M. Ivanov, Á. Jász, H. Ji, H. Jiang, B. Kaduk, S. Kähler, K. Khistyaev, J. Kim, G. Kis, P. Klunzinger, Z. Koczor-Benda, J. H. Koh, D. Kosenkov, L. Koulias, T. Kowalczyk, C. M. Krauter, K. Kue, A. Kunitsa, T. Kus, I. Ladjánszki, A. Landau, K. V. Lawler, D. Lefrancois, S. Lehtola, R. R. Li, Y.-P. Li, J. Liang, M. Liebenthal, H.-H. Lin, Y.-S. Lin, F. Liu, K.-Y. Liu, M. Loipersberger, A. Luenser, A. Manjanath, P. Manohar, E. Mansoor, S. F. Manzer, S.-P. Mao, A. V. Marenich, T. Markovich, S. Mason, S. A. Maurer, P. F. McLaughlin, M. F. S. J. Menger, J.-M. Mewes, S. A. Mewes, P. Morgante, J. W. Mullinax, K. J. Oosterbaan, G. Paran, A. C. Paul, S. K. Paul, F. Pavošević, Z. Pei, S. Prager, E. I. Proynov, Á. Rák, E. Ramos-Cordoba, B. Rana, A. E. Rask, A. Rettig, R. M. Richard, F. Rob, E. Rossomme, T. Scheele, M. Scheurer, M. Schneider, N. Sergueev, S. M. Sharada, W. Skomorowski, D. W. Small, C. J. Stein, Y.-C. Su, E. J. Sundstrom, Z. Tao, J. Thirman, G. J. Tornai, T. Tsuchimochi, N. M. Tubman, S. P. Veccham, O. Vydrov, J. Wenzel, J. Witte, A. Yamada, K. Yao, S. Yeganeh, S. R. Yost, A. Zech, I. Y. Zhang, X. Zhang, Y. Zhang, D. Zuev, A. Aspuru-Guzik, A. T. Bell, N. A. Besley, K. B. Bravaya, B. R. Brooks, D. Casanova, J.-D. Chai, S. Coriani, C. J. Cramer, G. Cserey, A. E. DePrince, R. A. DiStasio, A. Dreuw, B. D. Dunietz, T. R. Furlani, W. A. Goddard, S. Hammes-Schiffer, T. Head-Gordon, W. J. Hehre, C.-P. Hsu, T.-C. Jagau, Y. Jung, A. Klamt, J. Kong, D. S. Lambrecht, W. Liang, N. J. Mayhall, C. W. McCurdy, J. B. Neaton, C. Ochsenfeld, J. A. Parkhill, R. Peverati, V. A. Rassolov, Y. Shao, L. V. Slipchenko, T. Stauch, R. P. Steele, J. E. Subotnik, A. J. W. Thom, A. Tkatchenko, D. G. Truhlar, T. Van Voorhis, T. A. Wesolowski, K. B. Whaley, H. L. Woodcock, P. M. Zimmerman, S. Faraji, P. M. W. Gill, M. Head-Gordon, J. M. Herbert, and A. I. Krylov, "Software for the frontiers of quantum chemistry: An overview of developments in the Q-Chem 5 package," J. Chem. Phys. **155**, 084801 (2021).
[87]A. I. Krylov and P. M. W. Gill, "Q-Chem: An engine for innovation," WIREs Comput. Mol. Sci. **3**, 317 (2013).
[88]For more information on the PLÉIADES beamline see https://www.synchrotron-soleil.fr/en/beamlines/pleiades (Accessed on 07 November 2025).
[89]M. A. V. Ribeiro da Silva, L. M. P. F. Amaral, and P. Szterner, "Experimental study on the thermochemistry of 2-thiouracil, 5-methyl-2-thiouracil and 6-methyl-2-thiouracil," J. Chem. Thermodyn. **57**, 380 (2013).
[90]A. Szabo and N. S. Ostlund, *Modern Quantum Chemistry: Introduction to Advanced Electronic Structure Theory* (McGraw-Hill, New York, 1989).